pathway suggesting that this could be responsible for augmentation of HCV replication by miR-491.

2. Materials and methods

2.1. Cells, antibodies

The hepatoma-derived cell line Huh7 was maintained in DMEM supplemented with 10% FCS. The HCV subgenomic cell line Huh-RepSI, harboring HCV-N (genotype 1b), was previously described [8]. Antibodies to phospho-ERK (Thr202/Tyr204), Akt, phospho-Akt (Ser473) were purchased from Cell Signaling Technology. An antibody to β-actin (A-5441) was from Sigma–Aldrich. A mouse monoclonal antibody to HCV core protein (C7-50) was obtained from Affinity BioReagents. A mouse monoclonal antibody to HCV NS5A (clone 388) was from Meridian Life Science, Inc. LY294002, a PI3 kinase inhibitor, was obtained from Calbiochem.

2.2. Immunoblot analysis

Total cellular protein was extracted with lysis buffer containing 1% Nonidet P-40, 0.5% sodium deoxycholate, 0.1% SDS, 1 mM sodium vanadate, 50 mM NaF, and protease inhibitor cocktail (Nacalai Tesque, Japan) in phosphate-buffered saline. Protein samples were separated by SDS–polyacrylamide gel electrophoresis and transferred to a polyvinylidene difluoride membrane (Bio-Rad). After blocking, the membrane was probed with specific primary antibodies, followed by further incubation with a secondary antibody conjugated with horseradish peroxidase (GE Healthcare). Proteins were visualized using ECL Western blot detection reagents (GE Healthcare) and exposure to film.

2.3. miRNA transfection

Synthesized miRNAs, miR-192, miR-194, miR-215, miR-320, miR-491, and negative control miRNA were purchased from Thermo Fisher Scientific. Cells (2×10^5 per well) were seeded into 6-well plates, transfected with miRNA at a concentration of 10 nM using Lipofectamine RNAiMAX (Invitrogen) according to manufacturer's instruction. After incubation for 2 days, the cells were harvested and assayed by immunoblot or real-time RT-PCR analysis.

2.4. Dual luciferase assay

We used a dicistronic plasmid, pRLHL, to investigate the effects of miRNAs on HCV IRES (Fig. 2A) [9]. Huh7 cells (1×10^6 cells in a 10-cm dish) were transfected with 10 μg of pRLHL using FuGene6 (Roche). After 24 h, the cells were seeded into 24-well plates (5×10^4 cells per well) and transfected with miRNA or negative control at a concentration of 10 nM as described above. After incubation for 2 days, cells were lysed, and assayed for HCV IRES-dependent firefly luciferase activity and cap-dependent renilla luciferase activity using the Dual Luciferase Reporter Assay System (Promega).

2.5. Cell culture-infectious HCV

HJ3-5(YH/QL) is a chimeric cell culture-infectious virus with a genome consisting of the core to NS2 sequence of genotype 1a (H77) virus placed within the background of the genotype 2a JFH1 virus, and containing compensatory mutations in E1 (Y361H) and NS3 (Q1251L) [10]. Virus stock (10^7 focus-forming units (FFU)/ml) was prepared as described previously [11].

For HCV infection, Huh7 cells (2×10^5 per well) were seeded into 6-well plates. After overnight incubation, the medium was replaced with 1 ml medium containing 4×10^5 FFU virus (the infection was carried out at an m.o.i. of ~2). After 12 h incubation, the cells were washed with PBS and re-fed with normal culture medium. At 5 days after inoculation with the virus, total RNA was obtained from the cells using Trizol (Invitrogen).

2.6. Real-time reverse transcription-polymerase chain reaction (RT-PCR)

Total RNA was extracted from the cells with RNAeasy (QIAGEN). The RNA, 1 μg, was reverse transcribed with High Capacity RNA-to-cDNA Master Mix (Applied Biosystems) in a 20 μl reaction, then 1 μl of the reaction was subjected to real-time PCR assay using TaqMan Gene Expression Assays (Applied Biosystems).

2.7. Cell proliferation assay

Cell proliferation was assessed by WST-1 (2-[2-methoxy-4-nitrophenyl]-3-[4-nitrophenyl]-5-[2,4-disulpho-phenyl]-2H-tetrazolium, monosodium salt) assay according to the manufacturer's suggested protocol (Nacalai Tesque). Briefly, Huh7 cells (1×10^4 per well) were seeded into 96-well flat-bottom plates, transfected with synthesized miRNA or negative control as above, and cultured in DMEM containing 10% FBS. WST-1 reagent, 10 μl, was added to each well, the cells were incubated at 37 °C for 1 h, and absorbance at 450 nm was measured using a spectrophotometer.

2.8. miRNA array analysis

To screen for miRNA affected by HCV infection, we performed microarray analysis using *mir*Vana miRNA Bioarray V9.2 (Ambion), which carries genes for a total 633 kinds of miRNAs containing 471 human genes, 380 mouse genes and 238 rat genes. Using the flash PAGE system (Ambion), miRNA was purified from 22 μg total RNA extracted from HCVcc-infected cells or mock-infected cells. The purified miRNA samples from HCVcc-infected cells and mock-infected cells were labeled with Cy3 and Cy5, respectively, using mirVana miRNA Labeling kit (Ambion) and CyeDye Mono-Reactive Dye Pack (GE Healthcare Biosciences). The labeled miRNA was hybridized to the array for ~16 h at 42 °C. After hybridization, the array was washed with Low Stringency Wash (Ambion) once and High Stringency Wash (Ambion) twice. Next, the array was dried with centrifugation at 600*g* for 3 min and scanned with GenePix 4000B scanner (Axon Instruments, CA, USA). The signal data were calculated with an Array-Pro Analyzer ver. 4.5 (Media Cybernetics, Inc.). The array data were normalized by global normalization using the Microarray Data Analysis Tool (Filgen, Inc.).

3. Results

3.1. Identification of miRNAs regulated by HCV infection

Huh7 cells were infected with HCVcc at ~2 m.o.i. After incubation for 5 days, total RNA was extracted from the cells followed by purification with small RNA and miRNA array analysis. A portion of the cells was subjected to immunofluorescence analysis for staining of HCV core protein to verify that more than 90% of the cells were infected with HCV. The ratio of Cy3 intensity to Cy5 intensity was calculated and alteration of the miRNA expression profile was analyzed. A ratio of more than 1.5-fold increase/decrease was considered to be altered. To exclude miRNAs with low expression levels, those with a net intensity of Cy3 and Cy5 of more than 1000 were picked out. As a result, the miRNAs of miR-192, miR-194, miR-320, and miR-491 were identified as altered miRNAs (Table 1). miR-192 and miR-194 were up-regulated by HCV infection,

Table 1
miRNAs altered by HCV infection.

miRNA	Intensity				Sequence
	Cy3 (HCV)	Cy5 (mock)	Net	Cy3/Cy5	
miR-192	987.90	607.05	1594.95	1.63	CUGACCUAUGAAUUGACAGCC
miR-194	793.48	498.00	1291.48	1.59	UGUAACAGCAACUCCAUGUGGA
miR-215	156.21	69.39	225.60	2.25	AUGACCUAUGAAUUGACAGAC
miR-320	897.44	1401.93	2299.37	0.64	AAAAGCUGGGUUGAGAGGGCGAA
miR-491	925.38	2495.47	3420.85	0.37	AGUGGGGAACCCUUCCAUGAGGA

and miR-320 and miR-491 were down-regulated. In addition, miR-215, whose net expression while relatively low, was also studied in the subsequent investigation as an upregulated miRNA because it is considered to be a cousin of miR-192 (see their homologous sequences in Table 1). miR-215 showed a high induction level, and miR-192 and miR-215 were reported to have common induction mechanisms and target genes [12,13].

3.2. Regulation of HCV replication by miRNAs

Next, we checked whether the miRNAs were capable of regulating HCV replication. To assess this, we transfected Huh-RepSI, a HCV subgenomic replicon cell line, with synthesized miRNAs, and then monitored HCV RNA abundance and NS5A protein abundance using real-time RT-PCR and immunoblot analysis, respectively. Among the five miRNAs tested, miR-192/miR-215 and miR-491 significantly increased replicon abundance (Fig. 1A and B), while miR-194 and miR-320 did not show any significant change. HCV subgenomic replicon RNA contains the NS3 through NS5B region, which is required for genome RNA replication, but not for virus particle production. To confirm that the effect of the miRNAs was reproducible in a system equipped with the entire HCV life cycle, we used Huh7 cells infected with HCVcc. As expected, HCV abundance was upregulated by the three miRNAs in the HCVcc-infected cells similarly to HCV replicon cells (Fig. 1C and D). In addition, the HCV strain used in the experiment was a chimera of genotype 1a (H77, core to NS2) and genotype 2 (JFH-1, NS3 to NS5B) [10]. In particular, the genotype of the replication machinery of the virus (namely, NS3 to NS5B) was JFH-1. This differed from that of Huh-RepSI (HCV-N, genotype 1b) [8], which suggests that the enhancing effect of miR-192/miR-215 and miR-491 on HCV genome replication was not genotype-specific.

3.3. Effect of miRNAs on HCV IRES, cell proliferation

Since miR-192/miR-215 and miR-491 were shown to be capable of enhancing HCV replication, we next tried to elucidate how they regulate it. First, we examined whether the miRNAs can regulate HCV IRES activity. In this experiment, we transfected replicon cells with a dicistronic vector, pRLHL [9], which contained the firefly luciferase gene driven by HCV IRES and the renilla luciferase gene translated in a cap-dependent manner which was used as a control of general translational activity (Fig. 2A). After 24 h, the miRNAs were transfected, then luciferase activities induced by HCV IRES and cap translation were measured at 2 days after

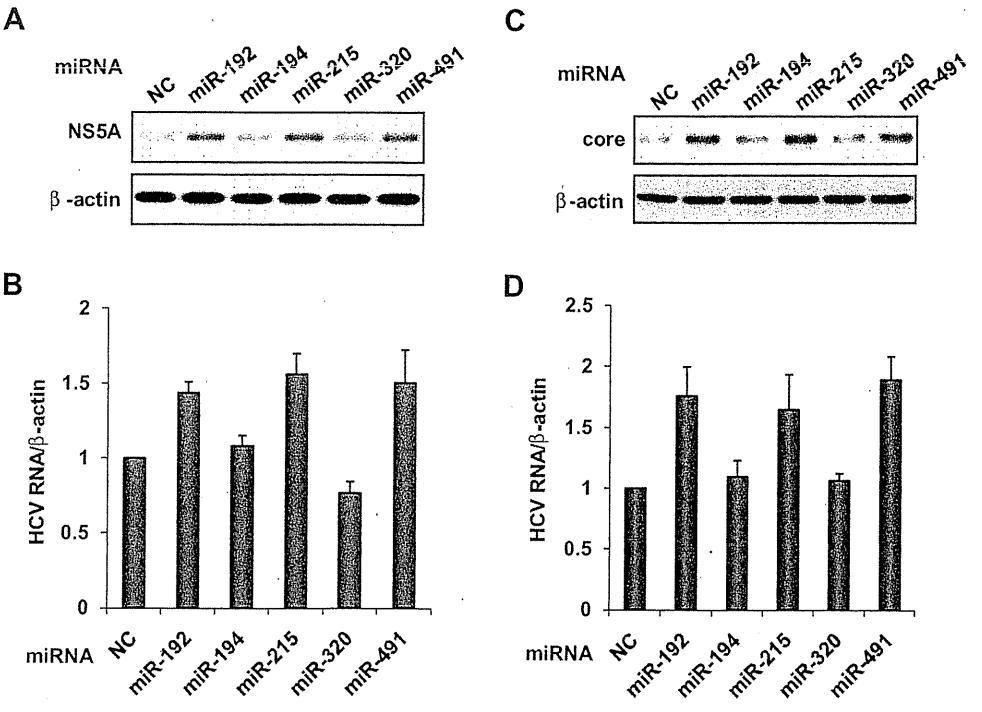

Fig. 1. Regulation of HCV replicon or HCVcc abundance by miRNAs. Cells of Huh-RepSI, a HCV subgenomic replicon, were transfected with synthesized miRNAs and assayed for NS5A protein expression (A) or HCV RNA abundance (B). HCVcc-infected Huh7 cells were transfected with synthesized miRNAs and assayed for core protein expression (C) or HCV RNA abundance (D). NC: negative control miRNA.

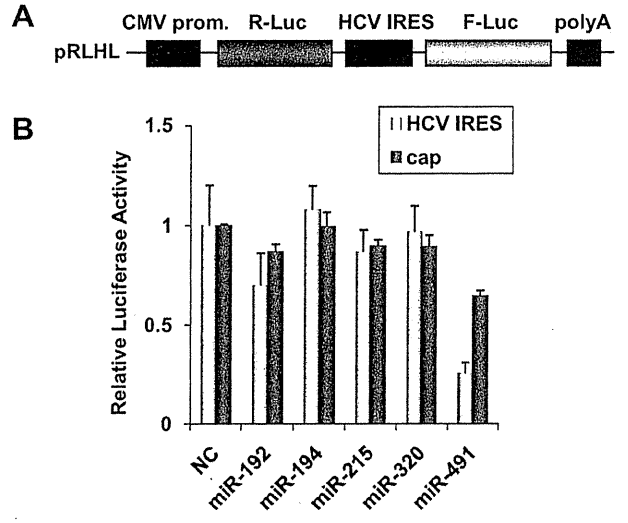

Fig. 2. Regulation of HCV IRES and cap-dependent translation by miRNAs. Huh-RepSI cells were transfected with a dicistronic vector, pRLHL (A), incubated for 24 h. The cells were seeded to 24-well plates and transfected with the miRNAs. After further incubation for 2 days, the cells were harvested and assayed for dual luciferase activity (B).

transfection (Fig. 2B). In this assay, activation of IRES was determined by the ratio of IRES-dependent luciferase activity to cap-dependent luciferase activity. Interestingly, none of the miRNAs could increase the HCV IRES activity. miR-491 suppressed cap-dependent translation and showed more suppression of HCV IRES activity. Thus, these results indicated that there was some mechanism upregulating HCV replication other than regulation of IRES activity.

Previous work demonstrated that HCV replication was affected by cell proliferation [14]. This led us to access the effects of the miRNAs on cell proliferation. Compared to negative control miRNA-transfected cells, however, none of the transfectants of the miRNAs, including those which increased HCV replication, revealed upregulation of cell proliferation, and miR-491 even suppressed it (Fig. 3). Therefore, regulation of cell proliferation was not the reason for the increase of HCV replication. The effect of miR-491 of suppressing cell growth was likely to be caused by inhibition of general translation as shown in Fig. 2B.

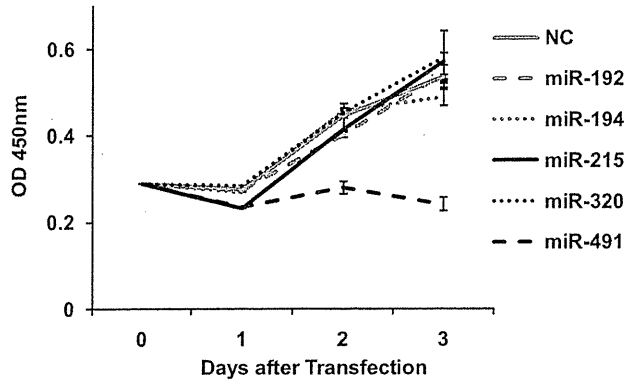

Fig. 3. Regulation of cell proliferation by miRNAs. Huh7 cells were seeded into 96-well plates, transfected with the miRNAs. At day 0, 1, 2, and 3 after transfection, the cells were subjected to WST-1 assay as described in Section 2.

3.4. Effect of miRNAs on intracellular signaling

To clarify the mechanism of the regulation of HCV replication, we next focused our investigation on intracellular signaling pathways. Previous studies have reported that HCV replication is regulated by intracellular signaling pathways, such as ERK [15], p38 [8], PI3 kinase/Akt [11], and smad [16], in addition to JAK/STAT. Since transfection of the miRNAs had no effect on the JAK/STAT signaling pathway (data not shown), we examined the phosphorylation of ERK and Akt. Because both showed a suppressing effect on HCV replication, suppression of the pathway was anticipated in cells in which HCV replication was enhanced. As shown in Fig. 4A, phosphorylation of Akt at Ser-473 was markedly suppressed in the cells transfected with miR-491, while no significant inhibition of ERK activity was observed. To further investigate the relevance of the PI3 kinase/Akt pathway to miR-491-induced upregulation of HCV replication, we used LY294002, a PI3 kinase inhibitor. When the PI3 kinase pathway was blocked by this reagent, the HCV RNA level was enhanced up to 2-fold. miR-491 transfection also resulted in an increase of HCV abundance, though the effect was less

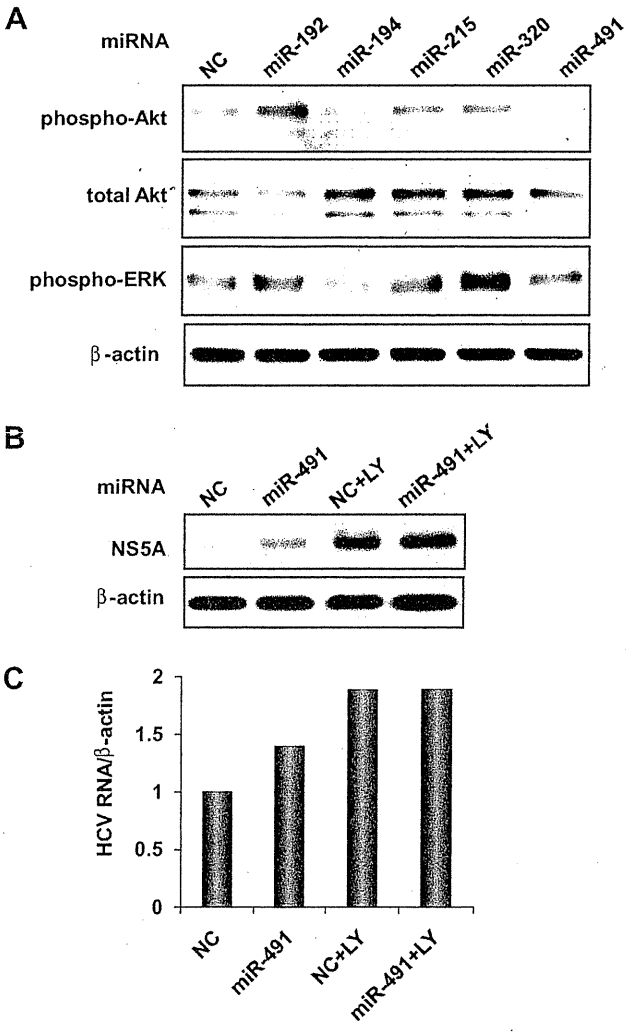

Fig. 4. Involvement of Akt suppression in miR-491-mediated upregulation of HCV replication. (A) Immunoblot analysis of miRNA-transfected HCV replicon cells using antibodies to Akt, phospho-Akt, phospho-ERK and β-actin. (B and C) HCV replicon cells were transfected with miR-491 or treated with Akt inhibitor, and assayed for NS5A protein abundance (B) or HCV RNA abundance (C). LY: LY294002.

than that of LY294002, presumably because of incomplete inhibition of Akt. When miR-491 transfected cells were cultured in the presence of LY294002, the HCV replication level was enhanced to the same extent as that in the LY294002-treated cells with negative control miRNA. Since no additive effect of miR-491 was observed under strong blockade of the PI3 kinase/Akt pathway, inhibition of this pathway was likely to be responsible for the miR-491-induced upregulation of HCV replication.

4. Discussion

In the present study, we tried to identify the miRNA(s) affected by HCV infection and establish how they influence HCV replication. Five miRNAs, miR-192, miR-194, miR-215, miR-320, and miR-491, were identified as HCV-regulated miRNAs by miRNA array analysis. Three upregulated miRNAs, miR-192, miR-194, and miR-215, were previously identified as p53-inducible miRNAs [12,13]. Two miRNA clusters which encode identical miR-194 sequences (i.e., the miR-194-2/miR-192 cluster on chromosome 11 and the miR-194-1/miR-215 cluster on chromosome 1) contain two closely related miRNAs, miR-192 and miR-215, suggesting that their expressions are regulated similarly which led to their simultaneous identification. miR-192/miR-194/miR-215 are known to act as tumor-suppressing miRNAs by inducing cell cycle arrest [12]. In Huh7 cells, however, the p53 function is believed to be abolished by a point mutation at codon 220. Therefore, the upregulation of miR-192/miR-194/miR-215 was likely to be exerted in a p53-independent manner. Since miR-192 and miR-194 are considered to be substantially expressed in human liver tissue [17] and there are several reports about the suppression of p53 function by HCV (reviewed in Ref. [18]), the result may not necessarily be the same if the investigation is conducted in human hepatocytes or in cells with intact p53 activity.

The downregulated miRNAs, miR-320 and miR-491, are considered to be relevant to carcinogenesis. miR-320 induces G1 arrest and suppresses cell proliferation by targeting CDK6 [19], CD71 [20], IGF1 [21] and induces apoptosis by suppressing Bcl-2 and Mcl-1 [22]. miR-491 is also capable of inducing apoptosis by targeting Bcl-xL [23], which is often upregulated in HCC tissues [24]. In this study, we showed that miR-491 inhibited the PI3 kinase/Akt pathway, which is one of the important pathways leading to cancerous properties. Importantly, miR-320 was identified as one of the significantly repressed miRNAs in CH-B, CH-C, and HCC compared with normal liver tissue [25]. Although the details of the relevance of miR320 and miR-491 to hepatocarcinogenesis have not yet been clarified, as these two miRNAs have a tendency to suppress genes related to carcinogenesis, their downregulation in HCV-infected cells may play some role in hepatocarcinogenesis.

Thus far, several miRNAs have been reported to regulate HCV replication. miR-122 was shown to be a direct activating factor for HCV replication [5], but alteration of this miRNA was not observed in response to HCV infection in this study. IFN-β-induced miRNAs, miR-196, miR-296, miR-351, miR-431 and miR-448, have been identified as anti-HCV miRNAs [6]. These miRNAs are able to regulate HCV replication by direct interaction with HCV genome RNA. In the case of miR-192/miR-215, there are several sites in the HCV genome sequence which show weak homology to the miRNAs (data not shown). Although the possibility of miR-192/miR-215 binding to the HCV genome and regulating replication cannot completely be excluded, this seems unlikely because the homologous sequence to miR-192/miR-215 cannot be found in the UTR region like miR-122 and direct binding to RNA usually suppresses the RNA function for protein synthesis. There is, however, a very rare case of miR-122-mediated facilitation of HCV replication by binding to two sites within the HCV genome.

Although the mechanism of miR-491-mediated suppression of the PI3 kinase pathway is not clear, it was speculated that some gene involved in Akt activation was the target of miR-491. However, the candidate of the target gene was not clearly found in the list of putative target genes of miR-491 revealed by in silico analysis. We tried to evaluate the mRNA levels of upstream genes of Akt, such as the genes which belong to the family of PI3 kinase, PTEN, growth factor receptors, using the RT-PCR method, but none of them was affected by miR-491 (data not shown). Nevertheless, investigation of target genes of miR-491 should be of interest for the field of oncology because here we have shown that miR-491 suppresses Akt, which is a factor closely related to various types of cancer via cell survival. Also, it has been demonstrated that miR-491 can induce apoptosis by ablating Bcl-xL [23]. Indeed, our observation that cell viability was significantly suppressed by forced expression of miR-491 presumably via decrease of Akt signaling suggests the anti-oncogenic feature of miR-491. Further study of the mechanism of miR-491, its target genes, and expression pattern in cancer tissue remain to be performed.

In conclusion, we showed altered expression profiles of miRNAs by HCV infection, and some of them were capable of regulating HCV replication, which may represent a complicated mechanism of HCV replication. A number of studies have demonstrated regulation of many cellular factors by miRNAs, which results in modulation of cellular functions including cell growth, apoptosis, cellular stresses, metabolism, and carcinogenesis. The miRNAs identified in this study may also be involved in changes in the phenotype of HCV-infected cells.

Acknowledgment

We thank Stanley Lemon for providing the plasmid pRLHL and the cell culture-infectious virus HJ3-5(YH/QL).

References

[1] L.B. Seeff, Natural history of hepatitis C, Hepatology 26 (1997) 21S–28S.
[2] M.W. Fried, M.L. Shiffman, K.R. Reddy, C. Smith, G. Marinos, F.L. Goncales Jr., D. Haussinger, M. Diago, G. Carosi, D. Dhumeaux, A. Craxi, A. Lin, J. Hoffman, J. Yu, Peginterferon alfa-2a plus ribavirin for chronic hepatitis C virus infection, N. Engl. J. Med. 347 (2002) 975–982.
[3] S.J. Hadziyannis, H. Sette Jr., T.R. Morgan, V. Balan, M. Diago, P. Marcellin, G. Ramadori, H. Bodenheimer Jr., D. Bernstein, M. Rizzetto, S. Zeuzem, P.J. Pockros, A. Lin, A.M. Ackrill, Peginterferon-alpha2a and ribavirin combination therapy in chronic hepatitis C: a randomized study of treatment duration and ribavirin dose, Ann. Intern. Med. 140 (2004) 346–355.
[4] M. Lagos-Quintana, R. Rauhut, W. Lendeckel, T. Tuschl, Identification of novel genes coding for small expressed RNAs, Science 294 (2001) 853–858.
[5] C.L. Jopling, M. Yi, A.M. Lancaster, S.M. Lemon, P. Sarnow, Modulation of hepatitis C virus RNA abundance by a liver-specific microRNA, Science 309 (2005) 1577–1581.
[6] I.M. Pedersen, G. Cheng, S. Wieland, S. Volinia, C.M. Croce, F.V. Chisari, M. David, Interferon modulation of cellular microRNAs as an antiviral mechanism, Nature 449 (2007) 919–922.
[7] K. Banaudha, M. Kaliszewski, T. Korolnek, L. Florea, M.L. Yeung, K.T. Jeang, A. Kumar, MicroRNA silencing of tumor suppressor DLC-1 promotes efficient hepatitis C virus replication in primary human hepatocytes, Hepatology 53 (2011) 53–61.
[8] H. Ishida, K. Ohkawa, A. Hosui, N. Hiramatsu, T. Kanto, K. Ueda, T. Takehara, N. Hayashi, Involvement of p38 signaling pathway in interferon-alpha-mediated antiviral activity toward hepatitis C virus, Biochem. Biophys. Res. Commun. 321 (2004) 722–727.
[9] T.H. Wang, R.C. Rijnbrand, S.M. Lemon, Core protein-coding sequence but not core protein modulates the efficiency of cap-independent translation directed by the internal ribosome entry site of hepatitis C virus, J. Virol. 74 (2000) 11347–11358.
[10] M. Yi, Y. Ma, J. Yates, S.M. Lemon, Compensatory mutations in E1 p7 NS2 and NS3 enhance yields of cell culture-infectious intergenotypic chimeric hepatitis C virus, J. Virol. 81 (2007) 629–638.
[11] H. Ishida, K. Li, M. Yi, S.M. Lemon, p21-activated kinase 1 is activated through the mammalian target of rapamycin/p70 S6 kinase pathway and regulates the replication of hepatitis C virus in human hepatoma cells, J. Biol. Chem. 282 (2007) 11836–11848.

[12] C.J. Braun, X. Zhang, I. Savelyeva, S. Wolff, U.M. Moll, T. Schepeler, T.F. Orntoft, C.L. Andersen, M. Dobbelstein, p53-Responsive micrornas 192 and 215 are capable of inducing cell cycle arrest, Cancer Res. 68 (2008) 10094–10104.
[13] S.A. Georges, M.C. Biery, S.Y. Kim, J.M. Schelter, J. Guo, A.N. Chang, A.L. Jackson, M.O. Carleton, P.S. Linsley, M.A. Cleary, B.N. Chau, Coordinated regulation of cell cycle transcripts by p53-Inducible microRNAs miR-192 and miR-215, Cancer Res. 68 (2008) 10105–10112.
[14] M. Honda, S. Kaneko, E. Matsushita, K. Kobayashi, G.A. Abell, S.M. Lemon, Cell cycle regulation of hepatitis C virus internal ribosomal entry site-directed translation, Gastroenterology 118 (2000) 152–162.
[15] T. Murata, M. Hijikata, K. Shimotohno, Enhancement of internal ribosome entry site-mediated translation and replication of hepatitis C virus by PD98059, Virology 340 (2005) 105–115.
[16] T. Murata, T. Ohshima, M. Yamaji, M. Hosaka, Y. Miyanari, M. Hijikata, K. Shimotohno, Suppression of hepatitis C virus replicon by TGF-beta, Virology 331 (2005) 407–417.
[17] O. Barad, E. Meiri, A. Avniel, R. Aharonov, A. Barzilai, I. Bentwich, U. Einav, S. Gilad, P. Hurban, Y. Karov, E.K. Lobenhofer, E. Sharon, Y.M. Shiboleth, M. Shtutman, Z. Bentwich, P. Einat, MicroRNA expression detected by oligonucleotide microarrays: system establishment and expression profiling in human tissues, Genome Res. 14 (2004) 2486–2494.
[18] M. Anzola, J.J. Burgos, Hepatocellular carcinoma: molecular interactions between hepatitis C virus and p53 in hepatocarcinogenesis, Expert Rev. Mol. Med. 5 (2003) 1–16.
[19] H. Duan, Y. Jiang, H. Zhang, Y. Wu, MiR-320 and miR-494 affect cell cycles of primary murine bronchial epithelial cells exposed to benzo[a]pyrene, Toxicol. In Vitro 24 (2010) 928–935.
[20] D.G. Schaar, D.J. Medina, D.F. Moore, R.K. Strair, Y. Ting, miR-320 targets transferrin receptor 1 (CD71) and inhibits cell proliferation, Exp. Hematol. 37 (2009) 245–255.
[21] X.H. Wang, R.Z. Qian, W. Zhang, S.F. Chen, H.M. Jin, R.M. Hu, MicroRNA-320 expression in myocardial microvascular endothelial cells and its relationship with insulin-like growth factor-1 in type 2 diabetic rats, Clin. Exp. Pharmacol. Physiol. 36 (2009) 181–188.
[22] L. Chen, H.X. Yan, W. Yang, L. Hu, L.X. Yu, Q. Liu, L. Li, D.D. Huang, J. Ding, F. Shen, W.P. Zhou, M.C. Wu, H.Y. Wang, The role of microRNA expression pattern in human intrahepatic cholangiocarcinoma, J. Hepatol. 50 (2009) 358–369.
[23] H. Nakano, T. Miyazawa, K. Kinoshita, Y. Yamada, T. Yoshida, Functional screening identifies a microRNA, miR-491 that induces apoptosis by targeting Bcl-X(L) in colorectal cancer cells, Int. J. Cancer 127 (2010) 1072–1080.
[24] T. Takehara, X. Liu, J. Fujimoto, S.L. Friedman, H. Takahashi, Expression and role of Bcl-xL in human hepatocellular carcinomas, Hepatology 34 (2001) 55–61.
[25] S. Ura, M. Honda, T. Yamashita, T. Ueda, H. Takatori, R. Nishino, H. Sunakozaka, Y. Sakai, K. Horimoto, S. Kaneko, Differential microRNA expression between hepatitis B and hepatitis C leading disease progression to hepatocellular carcinoma, Hepatology 49 (2009) 1098–1112.

Biochemical and Biophysical Research Communications 406 (2011) 614–620

Contents lists available at ScienceDirect

Biochemical and Biophysical Research Communications

journal homepage: www.elsevier.com/locate/ybbrc

Involvement of STAT3-regulated hepatic soluble factors in attenuation of stellate cell activity and liver fibrogenesis in mice

Minoru Shigekawa [a], Tetsuo Takehara [a,*], Takahiro Kodama [a], Hayato Hikita [a], Satoshi Shimizu [a], Wei Li [a], Takuya Miyagi [a], Atsushi Hosui [a], Tomohide Tatsumi [a], Hisashi Ishida [a], Tatsuya Kanto [a], Naoki Hiramatsu [a], Norio Hayashi [b]

[a] Department of Gastroenterology and Hepatology, Osaka University Graduate School of Medicine, Suita, Osaka, Japan
[b] Kansai Rosai Hospital, Amagasaki, Hyogo, Japan

ARTICLE INFO

Article history:
Received 19 February 2011
Available online 26 February 2011

Keywords:
STAT3
Liver fibrosis
Hepatic stellate cells
Acute phase proteins

ABSTRACT

Glycoprotein 130 (gp130)/signal transducer and activator of transcription 3 (STAT3) signaling in hepatocytes controls a variety of physiological and pathological processes including liver regeneration, apoptosis resistance and metabolism. Recent research has shed light on the importance of acute phase proteins (APPs) regulated by hepatic gp130/STAT3 in host defense through suppression of innate immune responses during systemic inflammation. To examine whether these STAT3-regulated soluble factors directly affect liver fibrogenic responses during liver injury, hepatocyte-specific STAT3 knockout (L-STAT3 KO) mice and control littermates were subjected to bile duct ligation (BDL) and examined 10 days later. In contrast to controls, L-STAT3 KO mice failed to produce APPs, such as serum amyloid A and haptoglobin, after BDL. Whereas L-STAT3 KO mice displayed similar levels of cholestasis, inflammatory cell infiltration and regeneration in the liver, they developed exacerbated liver injury and fibrosis with significant increases in expression of alpha-smooth muscle actin and type I collagen genes. *In vitro* experiments revealed that attenuated expression of APPs in primary hepatocytes isolated from L-STAT3 KO mice with IL-6 exposure, compared to wild-type hepatocytes. The cultured supernatant from IL-6-treated wild-type hepatocytes inhibited expression of alpha-smooth muscle actin and type I collagen genes in activated hepatic stellate cells (HSCs), whereas this did not occur with the supernatant from IL-6-treated knockout hepatocytes or with control medium. In conclusion, the absence of STAT3 in hepatocytes leads to exacerbation of liver fibrosis during cholestasis. Soluble factors released from hepatocytes, dependent on STAT3, collectively play a protective role in liver fibrogenesis through an inhibitory effect on activated HSCs.

1. Introduction

Cholestatic liver injury is characterized by bile flow impairment of different parts of the biliary tree, which can be caused by gallstones, autoimmunity or unknown etiology. Persistent cholestasis eventually progresses toward biliary fibrosis and cirrhosis because of bile acid-induced cholangiocyte and hepatocyte damage, leading to failure of cellular repopulation and excessive deposition of extracellular matrix (ECM) proteins. Hepatic stellate cells (HSCs) are the main ECM-producing cells in the injured liver [1]. Following chronic injury, HSCs activate or transdifferentiate into myofibroblast-like cells, acquiring contractile, proinflammatory and fibrogenic properties. Activated HSCs produce and deposit ECM proteins in the pericentral and periportal regions.

The signal transducer and activator of transcription 3 (STAT3) is known to be ubiquitously expressed in a wide range of tissues where it is activated by tyrosine phosphorylation in response to a variety of cytokines and growth factors (e.g. interleukin (IL)-6 family, IL-10, leptin, IL-17, IL-23, interferons and EGF). STAT3, formerly known as acute phase response factor, regulates the expression of genes involved in the acute phase response, a series of inflammatory reactions induced in response to infection and tissue

Abbreviations: ECM, extracellular matrix; HSCs, hepatic stellate cells; STAT, signal transducer and activator of transcription; IL, interleukin; gp, glycoprotein; APPs, acute phase proteins; L-STAT3 KO, hepatocyte-specific STAT3 knockout; WT, wild-type; BDL, bile duct ligation; TUNEL, terminal deoxynucleotidyl transferase-mediated deoxyuridine triphosphate nick-end labeling; BrdU, 5-bromo-2-deoxyuridine; rtPCR, reverse-transcription polymerase chain reaction; SAA, serum amyloid A; αSMA, alpha-smooth muscle actin; TGFβ, transforming growth factor beta; PDGF, platelet derived growth factor; ALT, alanine aminotransferase.

* Corresponding author. Address: Department of Gastroenterology and Hepatology, Osaka University Graduate School of Medicine, 2-2 Yamada-oka, Suita, Osaka 565-0871, Japan. Fax: +81 6 6879 3629.
E-mail address: takehara@gh.med.osaka-u.ac.jp (T. Takehara).

0006-291X/$ - see front matter © 2011 Elsevier Inc. All rights reserved.
doi:10.1016/j.bbrc.2011.02.105

injury [2]. The IL-6 family is one of the major cytokines involved in triggering the acute phase response and all members of the IL-6 family use glycoprotein 130 (gp130) as a receptor to induce nuclear translocation of STAT3 [3] as well as to activate the Ras/mitogen-activated protein (MAP) pathway. Since systemic deletion of STAT3 leads to embryonic lethality in mice, the significance of STAT3 in adult organs has been investigated using conditional knockout animals generated by the Cre/loxP recombination system [4]. Previous reports suggested that STAT3 signaling in hepatocytes controls a variety of physiological and pathological processes, including hepatocyte proliferation after partial hepatectomy [5], apoptosis resistance of hepatocytes during Fas-mediated liver injury [6] and regulation of hepatic gluconeogenic genes [7]. Further study showed that the soluble factors dependent on gp130/STAT3 signaling such as acute phase proteins (APPs) suppress innate immune cell overactivation and hypercytokinemia, leading to host-defense during systemic inflammation [8,9]. Very recently, research has shown that gp130/STAT3 signaling is protective against liver fibrogenesis by regulating inflammation and injury in the liver during chronic cholestasis [10,11]. However, it is not clear whether STAT3-dependent soluble factors from hepatocyte, such as APPs, affect the activation of HSCs and their collagen synthesis.

In the present study, we used conditional knockout mice, carrying hepatocyte-specific deletion of STAT3, and determined the effects dependent on the hepatocyte-specific STAT3 signaling pathway during cholestasis. We found that its signaling pathway offered protection from liver injury and fibrogenesis in a murine model of cholestatic liver injury. Moreover, STAT3-dependent soluble factors released from hepatocytes directly suppressed the activated HSCs and their collagen synthesis *in vitro*. Hepatocyte STAT3 signaling plays an important role in attenuation of liver disease by modulating liver damage and fibrogenesis through their collective effect on HSCs.

2. Materials and methods

2.1. Animals

Mice carrying a STAT3 gene with 2 loxP sequences flanking exon 22 have been described previously [12]. Hepatocyte-specific STAT3 knockout (L-STAT3 KO) mice were generated by crossing $STAT3^{fl/fl}$ mice with albumin-promoter Cre (Alb-Cre) transgenic mice [13]. Sex-matched $STAT3^{fl/fl}$ mice obtained from the same litter were used as wild-type (WT) controls. All mice were used at the age of 7–10 weeks. All animals were housed with 12-h light/dark cycles with free access to food and water under specific pathogen-free conditions and were treated with humane care under approval from the Animal Care and Use Committee of Osaka University Medical School.

2.2. Bile duct ligation

Bile duct ligation (BDL) is a well-established murine model of cholestasis. L-STAT3 KO mice and WT littermates were subjected to BDL as previously reported [14]. Briefly, the common bile duct was ligated 3 times with 5–0 silk sutures and then cut between the ligatures. After 10 days, the animals were sacrificed for the following analyses.

2.3. Histologic analyses

The liver sections were stained with H&E or picrosirius red. The percentage of oncotic necrosis or fibrotic area was calculated using image analysis software (win-ROOF visual system; Mitani Co., Tokyo, Japan). To assess intrahepatic macrophage accumulation, liver sections were stained with F4/80 using an anti-F4/80 rat monoclonal antibody (Abcam, Cambridge, MA). To detect apoptotic cells, the liver sections were also subjected to terminal deoxynucleotidyl transferase-mediated deoxyuridine triphosphate nick-end labeling (TUNEL) staining as previously reported [15]. To assess regenerative status, nuclear 5-bromo-2-deoxyuridine (BrdU) incorporation was evaluated as previously described [16].

2.4. Isolation and culture of murine hepatic stellate cells

HSCs were isolated from C57BL/6J mice by 2-step collagenase-pronase perfusion of mouse liver as previously described [16]. Activated HSCs after a few passages were cultured with the supernatant from primary hapatocyte or recombinant Apo-SAA (PEPROTECH, Rocky Hill, NJ).

2.5. Primary culture of hepatocytes

Hepatocytes were isolated from the liver of L-STAT3 KO mice and WT mice by 2-step collagenase-pronase perfusion of mouse liver as previously described [8]. Isolated hepatocytes were stimulated with 20 ng/ml recombinant mouse IL-6 (R&D Systems, Minneapolis, MN). The cells or the supernatant were harvested after 24 h.

2.6. Western blot analysis

Western blotting was performed as previously described [16].For immunodetection, the following antibodies were used: phospho-STAT3 (Tyr705) antibody, anti-STAT3 antibody (Cell Signaling Technology, Danvers, MA) and anti-β-actin antibody (Sigma–Aldrich, St. Louis, MO).

2.7. Real-time reverse-transcription polymerase chain reaction

Total RNA extracted from the liver tissue and HSCs were reverse transcribed and subjected to real-time reverse-transcription polymerase chain reaction (rtPCR) as previously described [15]. mRNA expression of the specific genes was quantified using TaqMan Gene Expression Assays (Applied Biosystems Inc., Foster City, CA). Assay IDs of the specific genes are provided in Supplementary Table 1. Transcript levels are presented as fold induction.

2.8. Enzyme-linked immunosorbent assay

The levels of serum amyloid A (SAA) and haptoglobin in serum and cultured supernatant were measured using SAA ELISA kit (Invitrogen, Camarillo, CA) and Mouse Haptoglobin ELISA kit (Immunology Consultants Laboratory, Newberg, OR), according to the manufacturer's protocol.

2.9. Statistical analysis

Data are presented as median and interquartile range or mean ± standard deviation, compared using the Mann–Whitney U test and unpaired *t*-test, respectively. Statistical significance was set at $p < 0.05$.

3. Results

3.1. Lack of acute phase response in L-STAT3 KO mice after BDL

L-STAT3 KO mice were produced by crossing floxed STAT3 mice and Alb-Cre transgenic mice which express Cre recombinase gene under regulation of the albumin gene promoter. To determine the

role of hepatocyte STAT3 during obstructive cholestasis, L-STAT3 KO mice and WT mice were subjected to BDL and examined 10 days later. After BDL treatment, western blot analysis revealed that STAT3 expression in the livers of L-STAT3 KO mice was greatly reduced compared with that of WT mice (Fig. 1A). In contrast to L-STAT3 KO mice, phosphorylation of STAT3 was clearly seen in WT mice with BDL compared with that in sham-operated mice (Fig. 1A). Given that STAT3 is a well-known mediator of APPs in the IL-6/gp130/STAT3 signaling pathway, we analyzed the mRNA expression of APPs such as SAA and haptoglobin by real-time rtPCR. The hepatic expression of SAA and haptoglobin genes was clearly induced after BDL in WT mice (Fig. 1B). In contrast, the hepatic expression of these genes did not increase in L-STAT3 KO mice. We also measured the serum levels of APPs. Similarly, the levels of SAA and haptoglobin clearly increased in WT littermates after BDL and were completely diminished in L-STAT3 KO mice (Fig. 1C).

3.2. L-STAT3 KO mice show progression of liver fibrosis

To examine the effect of hepatocyte-specific STAT3 deficiency on liver fibrosis after BDL, we evaluated hepatic collagen deposition by picrosirius red staining of liver sections (Fig. 2A). Morphometric analysis revealed that collagen deposition increased in both groups after BDL and was more significantly higher in L-STAT3 KO mice than in the WT littermates (Fig. 2B). As type I collagen is known to be a major form of collagen in cirrhosis, we analyzed hepatic expression of type I collagen α1 gene, *col1a1*. The levels more significantly increased in L-STAT3 KO mice than WT mice (Fig. 2C). HSCs are main collagen-producing cells in the injured liver and alpha-smooth muscle actin (αSMA) is the marker of activation of HSCs. The expression levels of αSMA gene, *acta2*, were significantly higher in L-STAT3 KO mice than WT controls after BDL (Fig. 2C). The mRNA expression of both transforming growth factor beta (TGFβ), as an important profibrogenic cytokine, and platelet derived growth factor (PDGF), which is the most potent mitogen for HSCs, were not significantly different between the two groups after BDL (Fig. 2D).

3.3. L-STAT3 KO mice display exacerbated liver injury

We examined liver injury and cholestasis upon BDL. There was no significant difference in cholestasis between the two groups after BDL as evidenced by serum levels of total bilirubin and alkaline phosphatase, but L-STAT3 KO mice showed increased levels of serum alanine aminotransferase (ALT) compared with WT controls (Fig. 3A). Oncotic necrosis, known as bile infarcts, is a characteristic feature of liver injury in the BDL model. The area of oncotic necrosis in the liver was not significantly different between the two groups after BDL (Fig. 3B). TUNEL staining of the liver sections revealed that the numbers of apoptotic cells in the liver more significantly increased in L-STAT3 KO mice than in WT littermates after BDL (Fig. 3C). We examined liver regeneration by BrdU incorporation in liver sections (Supplementary Fig. 1A). There was no significant difference between the two groups as determined by the count of BrdU-positive cells after BDL (Fig. 3D). Kupffer cells are resident macrophages that play a major role in liver inflammation by releasing cytokines. The F4/80 antigen is expressed on a wide range of mature tissue macrophages including Kupffer cells, and we thus examined F4/80 staining of liver sections (Supplementary Fig. 1B). There was no significant difference in the count of F4/80-positive cells between the two groups after BDL (Fig. 3E). The hepatic mRNA expression of CD68, expressed on monocytes/macrophages, CD4 and CD8, both of which are surface markers of T cells, was not significantly different between the two groups after BDL (Fig. 3F, Supplementary Fig. 2).

3.4. Soluble factors released from IL-6-treated hepatocytes are involved in suppression of activated HSCs and inhibition of their collagen production

In our *in vivo* study, we revealed the exacerbation of cholestasis-induced liver fibrosis and the increases in hepatic expression of αSMA and type I collagen α1 genes in L-STAT3 KO mice. Furthermore, the acute phase response induced after BDL was invisible in L-STAT3 KO mice. We hypothesized that STAT3-mediated soluble

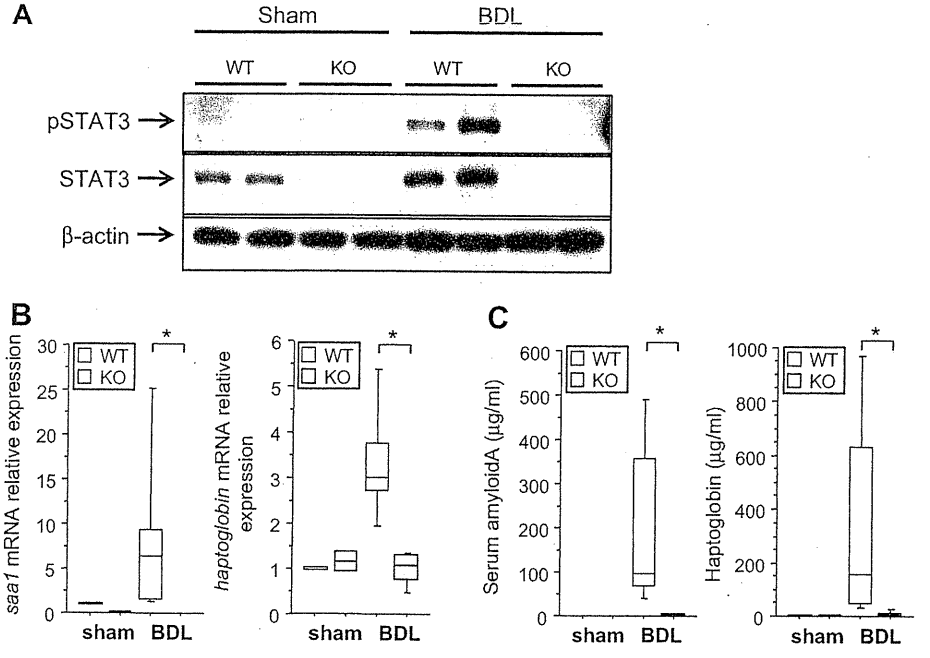

Fig. 1. Activation of STAT3 and production of acute phase proteins in the liver after BDL. L-STAT3 KO mice (KO) and WT littermates (WT) were subjected to BDL or sham-operation (sham) and examined 10 days later. (A) Expressions of STAT3 and phosphorylated STAT3 (pSTAT3) in the liver were assessed by western blot analysis. β-actin is included as a control. (B) Hepatic mRNA expression of SAA and haptoglobin was determined by real-time rtPCR analysis, $n = 8$/group, $^*p < 0.05$. (C) Serum levels of SAA and haptoglobin were determined by ELISA, $n = 8$/group, $^*p < 0.05$.

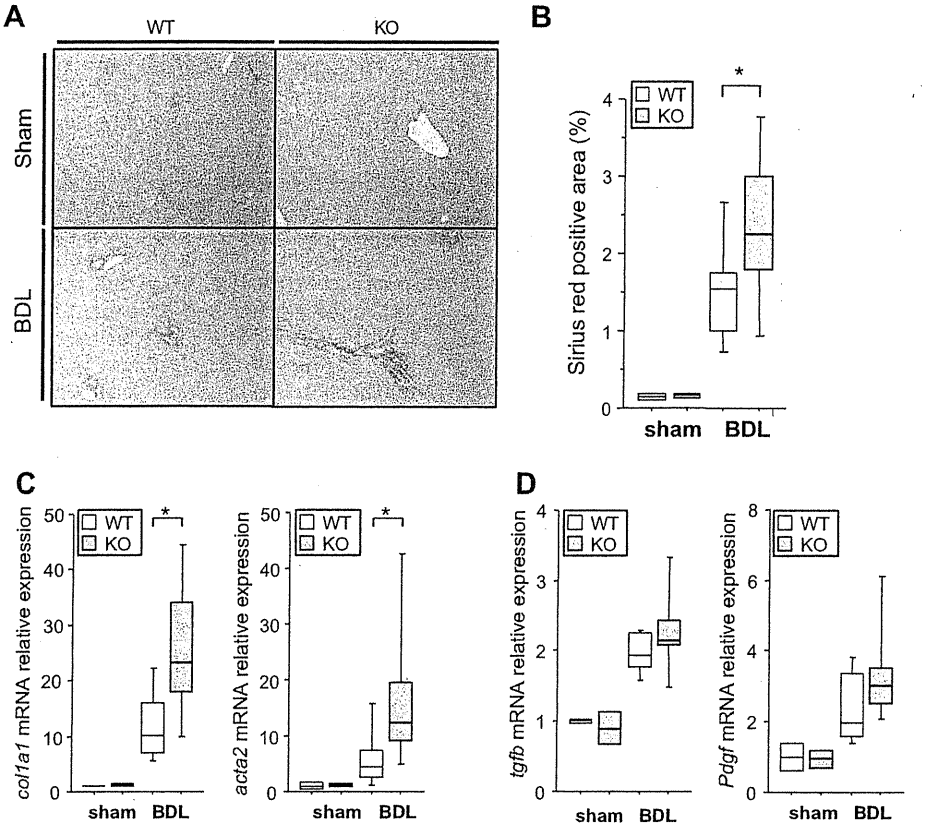

Fig. 2. Exacerbation of liver fibrosis in L-STAT3 KO mice after BDL. L-STAT3 KO mice (KO) and WT littermates (WT) were subjected to BDL or sham-operation (sham) and examined 10 days later. (A) Representative views of picrosirius red staining of the liver sections. (B) Morphometric analysis for picrosirius red staining, $n = 8$/group, $^*p < 0.05$. (C) Hepatic expression of αSMA and type I collagen α1 genes by real-time rtPCR analysis, $n = 8$/group, $^*p < 0.05$. (D) Hepatic expression of TGFβ and PDGF genes by real-time rtPCR analysis, $n = 8$/group.

factors released from hepatocytes repressed activated HSCs and their collagen synthesis. We isolated primary hepatocytes from L-STAT3 KO mice and WT controls, and stimulated them with or without IL-6. The cultured medium of stimulated hepatocytes was collected after 24 h. Whereas faint signals of STAT3 phosphorylation were observed under resting conditions in WT hepatocytes, administration of IL-6 clearly activated STAT3 phosphorylation in WT hepatocytes in contrast to STAT3 KO hepatocytes (Fig. 4A). Accordingly, IL-6 administration activated SAA and haptoglobin gene expression in WT hepatocytes, leading to production of higher levels of SAA and haptoglobin in culture supernatant compared with STAT3 KO hepatocytes (Fig. 4B, Supplementary Fig. 3).

Activated HSCs isolated from C57BL/6J were cultured with supernatant taken from IL-6-treated WT hepatocytes (sup-WT) or that from IL-6-treated STAT3 KO hepatocytes (sup-KO). Activated HSCs were also incubated with medium containing the same amount of IL-6 (sup-control) as a control. The mRNA expression of αSMA and type I collagen α1 in HSCs cultured with sup-WT significantly decreased compared with sup-control (Fig. 4C). On the other hand, the expression of these genes in HSCs cultured with sup-KO was similar to the levels of sup-control (Fig. 4C). In addition, activated HSCs were cultured with recombinant SAA. The expression of αSMA gene in HSCs decreased in dose-dependent manner, although the expression of type I collagen α1 gene did not change (Fig. 4D).

4. Discussion

Liver fibrosis is a consequence of chronic liver injury and inflammation. Accumulating evidence suggests that liver fibrosis is to some extent reversible by appropriate therapeutic intervention for chronic liver diseases [1]. Clarifying the cellular and molecular mechanisms involved in fibrogenesis and its progression has become very important for efficacious treatment. In the present study, we used L-STAT3 KO mice to examine the significance of this signaling pathway in liver fibrogenesis, because hepatocyte STAT3 is a crucial signaling transducer and transcription factor that regulates most, if not all, APPs which have been shown to possess a variety of biological properties during inflammation. We have demonstrated here that lack of STAT3 accelerates liver fibrosis during cholestasis and suggested that STAT3-dependent soluble factors collectively serve as a negative regulator for activation of HSCs.

Very recent research has shown that lack of gp130 or STAT3 in hepatocytes exacerbates liver fibrosis in murine sclerosis cholangitis models induced by 3,5-diethoxycarbonyl-1,4-dihydrocollidine (DDC) diet or genetic deletion of multidrug resistance gene 2 (*mdr2*), respectively. In those studies, deletion of gp130 or STAT3 induced severer cholestasis compared with control mice, leading to enhanced inflammatory cell infiltration and injury in the liver [10,11]. Therefore, exacerbation of liver fibrosis observed in those models might be ascribed to exacerbated cholestasis and liver

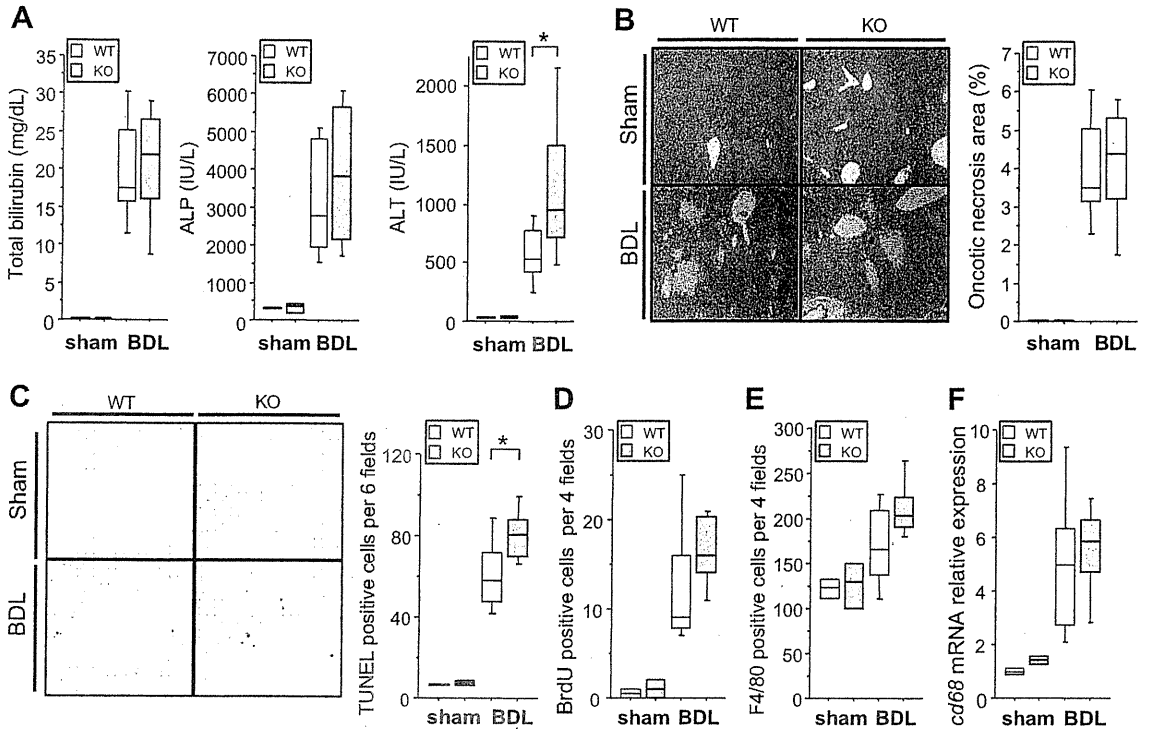

Fig. 3. Exacerbation of liver injury in L-STAT3 KO mice after BDL. L-STAT3 KO mice (KO) and WT littermates (WT) were subjected to BDL or sham-operation (sham) and examined 10 days later. (A) Serum levels of total bilirubin, alkaline phosphatase (ALP) and ALT, $n = 8$/group, $^*p > 0.05$. (B) Representative views of H&E staining of the liver sections and statistics for the area of oncotic necrosis determined by morphometric analysis of H&E staining, $n = 6$/group. (C) Representative views of TUNEL staining of the liver sections and statistics of TUNEL positive cells per 6 fields, $n = 8$/group. (D) The numbers of BrdU-positive cells of the liver sections, $n = 8$/group. 5-bromo-2-deoxyuridine (BrdU) was administered 2 h before sacrifice. (E) The numbers of F4/80-positive cells of the liver sections, $n = 8$/group. The liver sections were stained with anti-F4/80 antigen. (F) Hepatic mRNA expression of CD68 determined by real-time rtPCR analysis, $n = 8$/group.

inflammation. In the present study, we subjected our L-STAT3 KO mice to BDL, a well-established murine model of cholestasis, and examined them 10 days later. We found that hepatocyte-specific deletion of STAT3 promotes liver injury and fibrosis although the mice developed similar levels of cholestasis and inflammatory cell infiltration in the liver, compared with their control littermates. These results clearly indicated that hepatocyte STAT3 signaling negatively regulates liver fibrosis independently of cholestasis and inflammatory cell infiltration in our BDL model. An earlier study showed that deletion of the gp130 gene induced by Cre-mediated recombination under control of the Mx1 gene promoter exacerbated bacterial infection and increased mortality by 10 days after BDL, compared with control mice [17]. In our mice in which STAT3 had been deleted under control of the albumin gene promoter, no rise in mortality occurred after BDL. Since Mx1-Cre-mediated genetic recombination should occur not only in hepatocytes but also in other cell types including a variety of hematopoietic cells, the gp130/STAT3 signaling pathway of other cell types besides hepatocytes might have an impact on the infection control and survival after BDL.

L-STAT3 KO mice showed severer liver injury with increases in the levels of serum ALT and TUNEL-positive cells in the liver sections. This is consistent with the general concept that STAT3 promotes apoptosis resistance by regulating the expression of a variety of anti-apoptotic genes. Indeed previous research showed that the absence of hepatic STAT3 makes hepatocytes more vulnerable to Fas-mediated apoptosis [6]. In contrast to a previous finding that liver regeneration is suppressed in STAT3 KO mice after partial hepatectomy [5], compensatory regeneration after BDL did not differ between L-STAT3 KO mice and the control littermates. Accumulating evidence suggests that hepatocyte apoptosis promotes a liver fibrotic response via HSC activation. Kupffer cells and HSCs were reported to be able to engulf apoptotic bodies and to produce TNFα and TGFβ, respectively [18,19]. These cellular events may lead to the induction of profibrotic responses. Indeed, we previously reported that spontaneous apoptosis did induce mild fibrotic response with increased production of TGFβ *in vivo* [13]. In the present study, STAT3 KO mice displayed increased hepatic expression of αSMA and type I collagen α1 genes suggesting activation of HSCs after BDL, compared with WT controls. However, at the same time, there were no significant differences in the mRNA expression of proinflammatory cytokines such as TNFα (data not shown) and profibrogenic cytokines such as TGFβ and PDGF in the liver between the two groups. This suggested that other factors or cellular events except cytokines or apoptosis were involved in the difference of HSC activation between the two groups in our model.

APPs, defined as proteins whose serum levels change by >25% during inflammation, are mainly produced in the liver and regulated via gp130/STAT3 signaling [20]. Consistent with this, L-STAT3 KO mice showed impaired production of APPs in BDL. Recent research showed that APPs are regarded as important biological components of the immune response to infection and tissue injury [9,21]. The IL-6 family/gp130/STAT3 signaling pathway in hepatocytes regulates the acute phase response and the importance of this pathway during host defense has become evident recently. The present study demonstrated that the absence of STAT3 in hepatocytes during cholestasis led to progression of liver fibrosis as shown by collagen deposition and activation of HSCs. We investigated the direct influence of the soluble factors released from hepatocytes via STAT3 signaling on HSCs activation and collagen production *in vitro*. Interestingly, the mRNA expression of αSMA and type I collagen α1 significantly decreased in activated HSCs

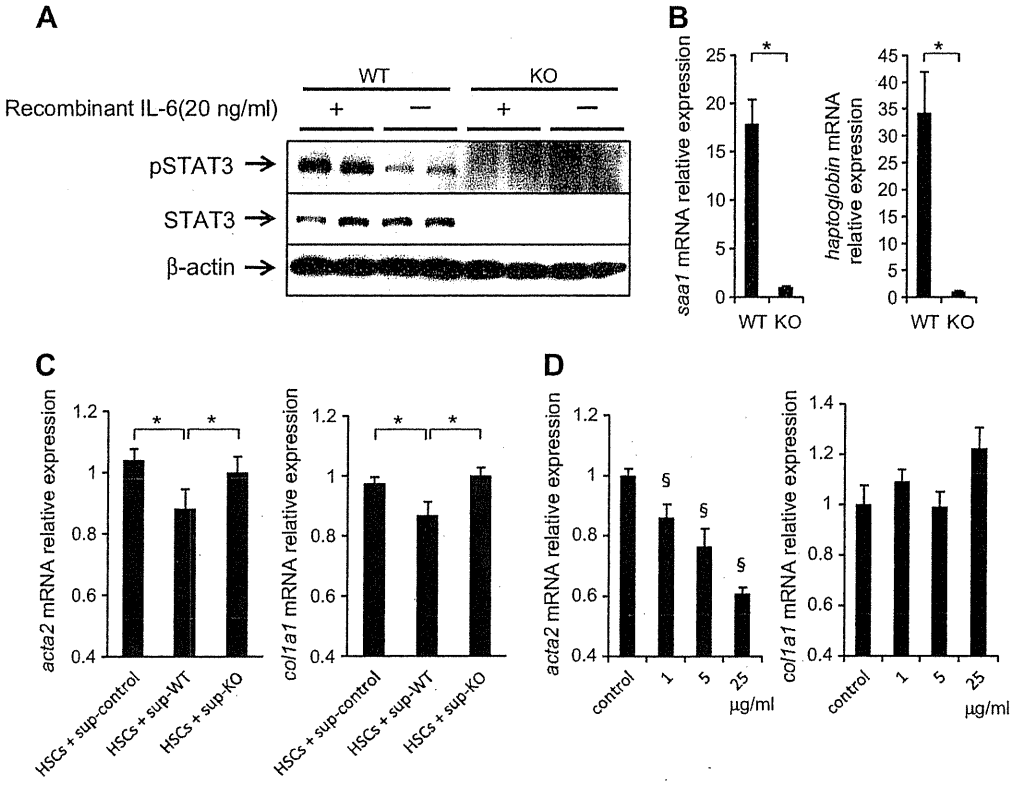

Fig. 4. Involvement of STAT3-dependent hepatic soluble factors in the suppression of activated HSCs. Primary hepatocytes isolated from L-STAT3 KO mice (KO) and WT mice (WT) were stimulated with or without 20 ng/ml of IL-6 for 24 h. (A) Expressions of STAT3 and pSTAT3 in hepatocytes by western blot analysis. β-actin is included as a control. (B) Real-time rtPCR analysis of mRNA expression of SAA and haptoglobin in IL-6-treated hepatocytes, $n = 4$/group, $^{*}p < 0.05$. (C) Real-time rtPCR analysis of αSMA and type I collagen α1 mRNA expression in HSCs, $n = 4$/group, $^{*}p < 0.05$. Activated HSCs were cultured for 24 h with control medium (sup-control), the cultured supernatant from WT hepatocytes (sup-WT) or that from STAT3 KO hepatocytes (sup-KO), stimulated with 20 ng/ml IL-6, respectively. (D) Real-time rtPCR analysis of αSMA and type I collagen α1 mRNA expression in HSCs, $n = 4$/group, $^{§}p < 0.05$ vs the other three groups. Activated HSCs were cultured with recombinant SAA (0, 1, 5, 25 μg/ml) for 24 h.

cultured with sup-WT compared with control medium. In contrast, the expression levels of these genes in activated HSCs remained unchanged when cultured with sup-KO. Since Sup-WT was abundant with SAA and haptoglobin, these findings imply that the hepatocyte STAT3-dependent soluble factors, such as APPs, directly repressed activated HSCs and their collagen production. Indeed, SAA negatively regulated HSC activation, although the mRNA expression of type I collagen α1 was unchanged, providing an example among APPs being able to downregulate activation marker of HSCs. Although further study is needed, the present study suggested that APPs could collectively inhibit HSC activity and collagen production.

In conclusion, the present study demonstrated that the absence of STAT3 in hepatocytes exacerbated liver injury and fibrosis during cholestasis. We speculated that both increase in hepatocyte apoptosis and lack of an acute phase response may contribute to accelerated liver fibrosis in this model. APPs had been individually analyzed to have pro- and anti-inflammatory properties during inflammation. The current study unveiled a previously unrecognized role of STAT3-dependent hepatic APPs in collectively serving as a negative regulator for HSC activation.

Acknowledgments

We thank Dr. S. Akira and Dr. K. Takeda for providing STAT3 floxed mice. This work was supported by a Grant-in-Aid for Scientific Research from the Ministry of Education, Culture, Sports, Science, and Technology, Japan.

Appendix A. Supplementary data

Supplementary data associated with this article can be found, in the online version, at doi:10.1016/j.bbrc.2011.02.105.

References

[1] R. Bataller, D.A. Brenner, Liver fibrosis, J. Clin. Invest. 115 (2005) 209–218.
[2] S. Akira, Y. Nishio, M. Inoue, et al., Molecular cloning of APRF, a novel IFN-stimulated gene factor 3 p91-related transcription factor involved in the gp130-mediated signaling pathway, Cell 77 (1994) 63–71.
[3] T. Taga, T. Kishimoto, Gp130 and the interleukin-6 family of cytokines, Annu. Rev. Immunol. 15 (1997) 797–819.
[4] K. Takeda, K. Noguchi, W. Shi, et al., Targeted disruption of the mouse STAT3 gene leads to early embryonic lethality, Proc. Natl. Acad. Sci. USA 94 (1997) 3801–3804.
[5] W. Li, X. Liang, C. Kellendonk, et al., STAT3 contributes to the mitogenic response of hepatocytes during liver regeneration, J. Biol. Chem. 277 (2002) 28411–28417.
[6] S. Haga, K. Terui, H.Q. Zhang, et al., Stat3 protects against Fas-induced liver injury by redox-dependent and -independent mechanisms, J. Clin. Invest. 112 (2003) 989–998.
[7] H. Inoue, W. Ogawa, M. Ozaki, et al., Role of STAT-3 in regulation of hepatic gluconeogenic genes and carbohydrate metabolism in vivo, Nat. Med. 10 (2004) 168–174.
[8] R. Sakamori, T. Takehara, C. Ohnishi, et al., Signal transducer and activator of transcription 3 signaling within hepatocytes attenuates systemic inflammatory response and lethality in septic mice, Hepatology 46 (2007) 1564–1573.
[9] L.E. Sander, S.D. Sackett, U. Dierssen, et al., Hepatic acute-phase proteins control innate immune responses during infection by promoting myeloid-derived suppressor cell function, J. Exp. Med. 207 (2010) 1453–1464.
[10] W. Plum, D.F. Tschaharganeh, D.C. Kroy, et al., Lack of glycoprotein 130/signal transducer and activator of transcription 3-mediated signaling in hepatocytes

enhances chronic liver injury and fibrosis progression in a model of sclerosing cholangitis, Am. J. Pathol. 176 (2010) 2236–2246.
[11] M. Mair, G. Zollner, D. Schneller, et al., Signal transducer and activator of transcription 3 protects from liver injury and fibrosis in a mouse model of sclerosing cholangitis, Gastroenterology 138 (2010) 2499–2508.
[12] K. Takeda, T. Kaisho, N. Yoshida, et al., Stat3 activation is responsible for IL-6-dependent T cell proliferation through preventing apoptosis: generation and characterization of T cell-specific STAT3-deficient mice, J. Immunol. 161 (1998) 4652–4660.
[13] T. Takehara, T. Tatsumi, T. Suzuki, et al., Hepatocyte-specific disruption of Bcl-xL leads to continuous hepatocyte apoptosis and liver fibrotic responses, Gastroenterology 127 (2004) 1189–1197.
[14] J. Kountouras, B.H. Billing, P.J. Scheuer, Prolonged bile duct obstruction: a new experimental model for cirrhosis in the rat, Br. J. Exp. Pathol. 65 (1984) 305–311.
[15] H. Hikita, T. Takehara, S. Shimizu, et al., The Bcl-xL inhibitor, ABT-737, efficiently induces apoptosis and suppresses growth of hepatoma cells in combination with sorafenib, Hepatology 52 (2010) 1310–1321.
[16] T. Kodama, T. Takehara, H. Hikita, et al., Thrombocytopenia exacerbates cholestasis-induced liver fibrosis in mice, Gastroenterology 138 (2010) 2487–2498.
[17] T. Wuestefeld, C. Klein, K.L. Streetz, et al., Lack of gp130 expression results in more bacterial infection and higher mortality during chronic cholestasis in mice, Hepatology 42 (2005) 1082–1090.
[18] A. Canbay, A.E. Feldstein, H. Higuchi, et al., Kupffer cell engulfment of apoptotic bodies stimulates death ligand and cytokine expression, Hepatology 38 (2003) 1188–1198.
[19] A. Canbay, P. Taimr, N. Torok, et al., Apoptotic body engulfment by a human stellate cell line is profibrogenic, Lab. Invest. 83 (2003) 655–663.
[20] C. Gabay, I. Kushner, Acute-phase proteins and other systemic responses to inflammation, N. Engl. J. Med. 340 (1999) 448–454.
[21] M. Luchtefeld, H. Schunkert, M. Stoll, et al., Signal transducer of inflammation gp130 modulates atherosclerosis in mice and man, J. Exp. Med. 204 (2007) 1935–1944.

Increases in p53 expression induce CTGF synthesis by mouse and human hepatocytes and result in liver fibrosis in mice

Takahiro Kodama,[1] Tetsuo Takehara,[1] Hayato Hikita,[1] Satoshi Shimizu,[1] Minoru Shigekawa,[1] Hinako Tsunematsu,[1] Wei Li,[1] Takuya Miyagi,[1] Atsushi Hosui,[1] Tomohide Tatsumi,[1] Hisashi Ishida,[1] Tatsuya Kanto,[1] Naoki Hiramatsu,[1] Satoshi Kubota,[2] Masaharu Takigawa,[2] Yoshito Tomimaru,[3] Akira Tomokuni,[3] Hiroaki Nagano,[3] Yuichiro Doki,[3] Masaki Mori,[3] and Norio Hayashi[4]

[1]Department of Gastroenterology and Hepatology, Osaka University Graduate School of Medicine, Suita, Osaka, Japan. [2]Department of Biochemistry and Molecular Dentistry, Okayama University Graduate School of Medicine, Dentistry and Pharmaceutical Sciences, Okayama, Japan. [3]Department of Surgery, Osaka University Graduate School of Medicine, Suita, Osaka, Japan. [4]Kansai-Rosai Hospital, Amagasaki, Hyogo, Japan.

The tumor suppressor p53 has been implicated in the pathogenesis of non-cancer-related conditions such as insulin resistance, cardiac failure, and early aging. In addition, accumulation of p53 has been observed in the hepatocytes of individuals with fibrotic liver diseases, but the significance of this is not known. Herein, we have mechanistically linked p53 activation in hepatocytes to liver fibrosis. Hepatocyte-specific deletion in mice of the gene encoding Mdm2, a protein that promotes p53 degradation, led to hepatocyte synthesis of connective tissue growth factor (CTGF; the hepatic fibrogenic master switch), increased hepatocyte apoptosis, and spontaneous liver fibrosis; concurrent removal of *p53* completely abolished this phenotype. Compared with wild-type controls, mice with hepatocyte-specific *p53* deletion exhibited similar levels of hepatocyte apoptosis but decreased liver fibrosis and hepatic CTGF expression in two models of liver fibrosis. The clinical significance of these data was highlighted by two observations. First, p53 upregulated CTGF in a human hepatocellular carcinoma cell line by repressing miR-17-92. Second, human liver samples showed a correlation between CTGF and p53-regulated gene expression, which were both increased in fibrotic livers. This study reveals that p53 induces CTGF expression and promotes liver fibrosis, suggesting that the p53/CTGF pathway may be a therapeutic target in the treatment of liver fibrosis.

Introduction

The tumor suppressor p53 primarily functions as a guardian of the genome, suppressing tumor development in various organs. In response to genotoxic stresses induced by DNA damage, reactive oxygen species, oncogene activation, and hypoxia, the p53 protein is stabilized and becomes transcriptionally active, leading to cell cycle arrest, DNA repair, and apoptosis predominantly through expression of p53-regulated genes such as *p21*, *PUMA*, *NOXA*, and *BAX* (1). Aside from these well-established roles, recent reports have revealed new aspects of p53, e.g., regulation of multiple biological functions such as glycolysis (2), anti-oxidation (3), autophagy (4), and senescence (5). It has also been demonstrated that p53 activation causes insulin resistance (6), cardiac failure (7), and early aging (5), indicating that p53 is involved even in the pathophysiology of various non-tumorous conditions via its numerous functions.

Organ fibrosis is considered to be a major medical issue, as various organs are involved, such as the liver, lung, heart, kidney, and skin, and its progression leads to organ failure and, especially in the liver, tumor development. The molecular mechanism of organ fibrosis has not yet been comprehensively clarified due to its complexity, and thus far, whether p53 is directly involved in its pathophysiology has not been addressed. Recently, p53 has been shown to accumulate in hepatocytes of several fibrotic liver diseases, such as non-alcoholic steatohepatitis (NASH) (8, 9), viral hepatitis (10, 11), and primary biliary cirrhosis (PBC) (12). However, the precise role of p53 in liver fibrosis is unclear. To this end, in the present study, we generated mice with hepatocyte-specific deletion of *Mdm2*, a critical p53 inhibitor, which strictly maintains p53 at a low level by promoting p53 degradation via the ubiquitin/proteasome pathway (13). Studies in these mice revealed that hepatocyte p53 activation caused spontaneous liver fibrosis. In addition to increased hepatocyte apoptosis, these mice showed hepatocyte upregulation of connective tissue growth factor (CTGF), known to be the fibrogenic master switch in fibrotic liver diseases (14). In vitro study revealed that p53 induced CTGF synthesis in hepatocytes via microRNA (miRNA) regulation. Hepatocyte-specific knockdown of *p53* attenuated CTGF expression and liver fibrosis induced by an atherogenic (ATH) diet or TAA injection. In human liver samples, p53-regulated gene expression increased in the fibrotic liver in correlation with an increase in *CTGF* gene expression. These findings demonstrated for the first time to our knowledge that p53 is directly involved in fibrogenesis in association with the induction of profibrogenic gene expression, suggesting that hepatocyte p53 activation and subsequent CTGF upregulation could be therapeutic targets in fibrotic liver disease.

Results

Hepatocyte-specific Mdm2 deficiency causes endogenous p53 accumulation, leading to transactivation of p53-regulated genes. To investigate the role of p53 in liver fibrosis, we first generated hepatocyte-specific Mdm2-knockout mice by crossing *Mdm2* floxed mice (*Mdm2*$^{fl/fl}$)

Authorship note: Takahiro Kodama and Tetsuo Takehara contributed equally to this work and share first authorship.

Conflict of interest: The authors have declared that no conflict of interest exists.

Citation for this article: *J Clin Invest.* 2011;121(8):3343–3356. doi:10.1172/JCI44957.

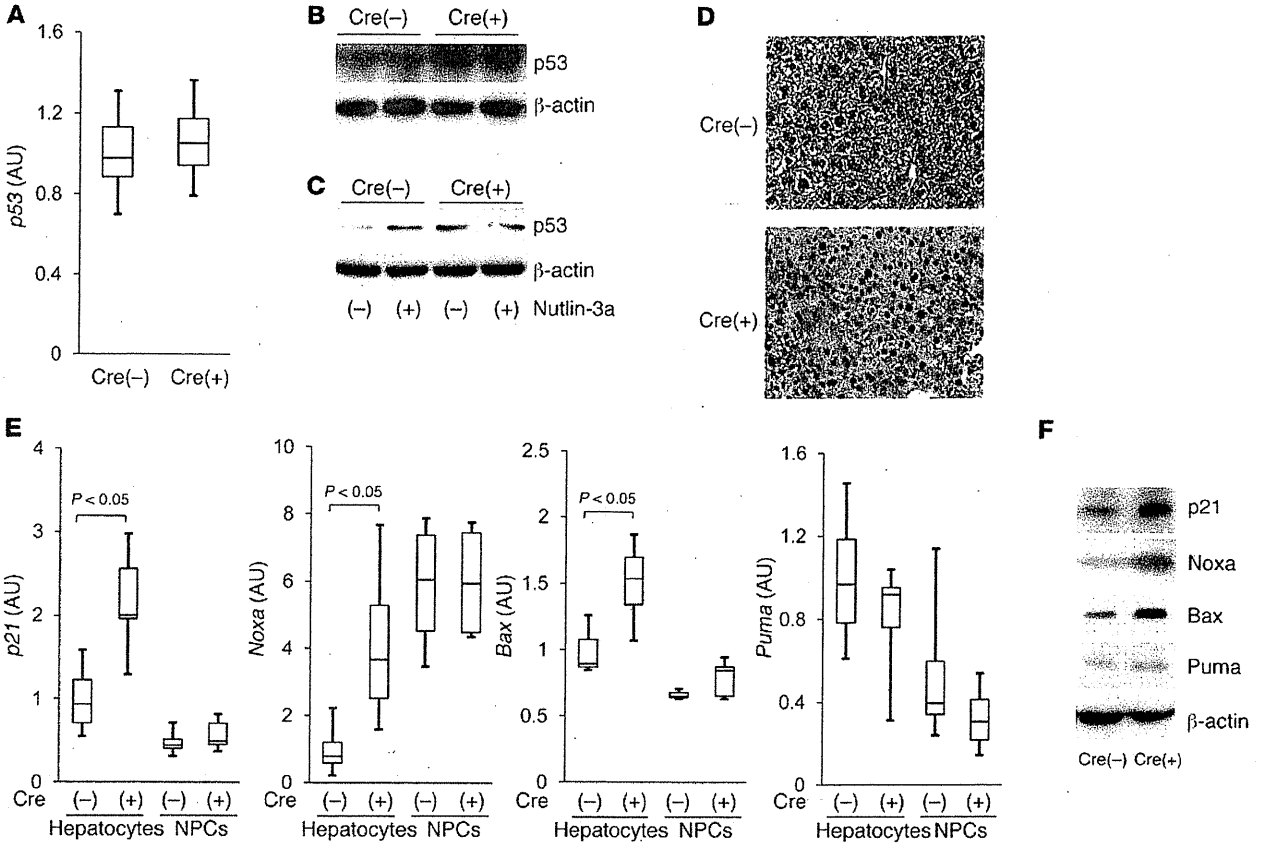

Figure 1

Hepatocyte-specific Mdm2-knockout mice show endogenous p53 accumulation, leading to transactivation of p53-regulated genes. (**A–F**) *Mdm2*$^{fl/fl}$*alb-cre* [Cre(+)] mice and *Mdm2*$^{fl/fl}$ [Cre(–)] mice were analyzed at 6 weeks of age. (**A**) *p53* mRNA levels in the liver tissue were determined by real-time RT-PCR; 7 mice per group. (**B**) Expression of p53 protein in liver tissue was assessed by Western blot analysis. (**C**) Expression of p53 protein in isolated hepatocytes upon treatment with 20 μM nutlin-3a or vehicle was assessed by Western blot analysis. (**D**) Expression of p53 protein in the liver section was determined by immunohistochemical analysis. Original magnification, ×200. (**E**) *p21*, *Noxa*, *Bax*, and *Puma* mRNA levels in isolated hepatocytes and NPCs were determined by real-time RT-PCR; 4 mice per group. Expression of p21, Noxa, Bax, and Puma proteins in liver tissue was assessed by Western blot analysis (**F**).

(15) and Alb-Cre transgenic mice (*alb-cre*) (16). After mating of *Mdm2*$^{fl/+}$*alb-cre* mice with *Mdm2*$^{fl/+}$ mice, *Mdm2*$^{fl/fl}$*alb-cre* mice were born at the expected Mendelian frequency and grew normally (Supplemental Figure 1; supplemental material available online with this article; doi:10.1172/JCI44957DS1). Next, we bred the *Mdm2*$^{fl/fl}$*alb-cre* mice with the *Mdm2*$^{fl/fl}$ mice and used *Mdm2*$^{fl/fl}$*alb-cre* mice as the knockout mice and *Mdm2*$^{fl/fl}$ mice as control littermates in the subsequent experiments. We examined whether Mdm2 deficiency would cause p53 accumulation in the liver. Real-time RT-PCR study revealed that hepatic levels of *p53* mRNA were not significantly different in the knockout mice and the control littermates (Figure 1A). Western blot analysis showed that hepatic p53 protein increased in the knockout mice compared with control littermates (Figure 1B). To determine whether an increase in p53 occurs in hepatocytes, we isolated hepatocytes from the liver by the collagenase-pronase perfusion procedure (17) and then examined their expression of p53 protein. Western blot analysis showed that the levels of hepatocyte p53 protein were higher in the knockout mice than in the control littermates (Figure 1C). These findings indicated that hepatocyte-specific Mdm2-knockout mice exhibited accumulation of p53 protein in their hepatocytes independent of the transcriptional upregulation of the *p53* gene. In addition, p53 expression increased in hepatocytes isolated from the control littermates, but not from the knockout mice, upon treatment with nutlin-3a, a small molecule Mdm2 inhibitor that blocks p53-Mdm2 interaction (ref. 18 and Figure 1C). This result demonstrated that lack of the Mdm2 function in hepatocytes of the knockout mice led to accumulation of endogenous p53 protein. Immunohistochemical examination of the liver sections revealed that p53 protein had accumulated in hepatocytes of the knockout mice, with some nuclear localization (Figure 1D), suggesting that p53 may become functionally active in hepatocytes of the knockout mice. This led us to investigate whether the p53 accumulation would lead to transactivation of p53-regulated genes *p21*, *Noxa*, *Bax*, and *Puma*. Real-time RT-PCR study revealed that, among these genes, the expression levels of *p21*, *Noxa*, and *Bax* was significantly higher in hepatocytes of the knockout mice than the control littermates (Figure 1E). Western blot study demonstrated that protein levels of these p53-regulated genes increased in the knockout mice as well (Figure 1F). These results demonstrated that hepatocyte-specific *Mdm2* deletion led to p53 accumulation and caused functional activation of p53 in hepatocytes.

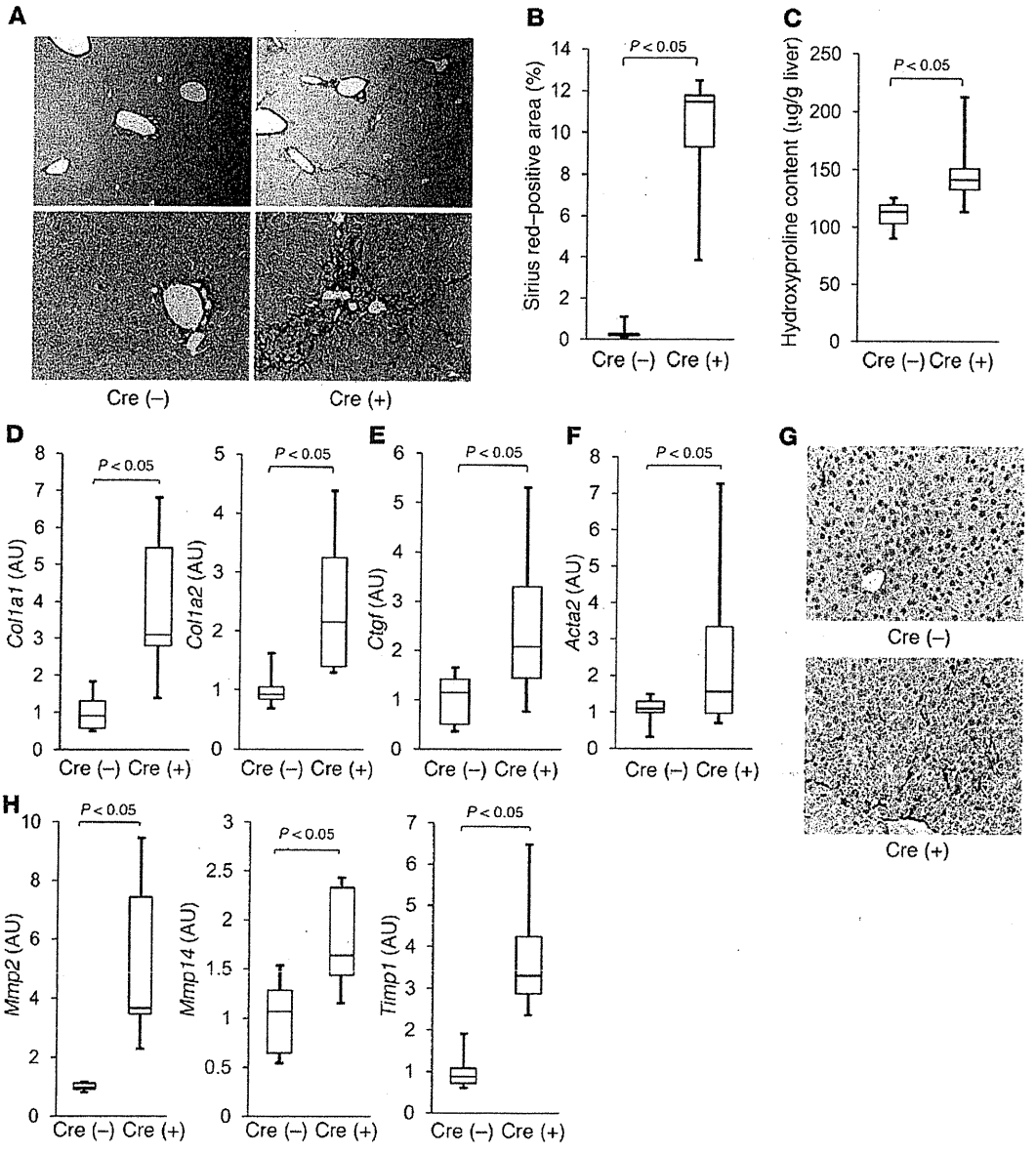

Figure 2

Hepatocyte-specific Mdm2-knockout mice develop spontaneous liver fibrosis with an increase in expression of the *Ctgf* gene. (**A–H**) *Mdm2*$^{fl/fl}$*alb-cre* [Cre(+)] mice and *Mdm2*$^{fl/fl}$ [Cre(–)] mice were analyzed at 6 weeks of age; 6 mice per group. (**A**) Liver fibrosis was evaluated by picrosirius red staining of liver sections (original magnification, upper panels, ×100; lower panels, ×200). (**B**) Sirius red–positive area of liver sections. (**C**) Hepatic hydroxyproline content. *Col1a1* and *Col1a2* (**D**), *Ctgf* (**E**), and *Acta2* (**F**) mRNA levels in the liver were determined by real time RT-PCR. (**G**) Expression of α-SMA in the liver sections was analyzed by immunohistochemistry. Original magnification, ×200. (**H**) *Mmp2*, *Mmp14*, and *Timp1* mRNA levels in the liver were determined by real time RT-PCR.

Hepatocyte-specific Mdm2-knockout mice develop spontaneous liver fibrosis with an increase in Ctgf gene expression. We next examined the consequences of hepatocyte p53 activation in the liver of Mdm2-knockout mice. To assess liver fibrosis, we evaluated hepatic collagen deposition by picrosirius red staining of liver tissues. At 6 weeks of age, pericellular and periportal bridging fibrosis was observed in liver of the knockout mice (Figure 2A), and it persisted even at a later time point (Supplemental Figure 2). Their collagen deposition significantly increased compared with that in the control littermates (Figure 2B). Hepatic hydroxyproline content, a biochemical marker of collagen accumulation (16), was also significantly higher in the knockout mice than in the wild-type mice (Figure 2C). We examined hepatic expression of the type I collagen genes *Col1a1* and *Col1a2* and found it to be significantly higher in the knockout mice than in the control littermates (Figure 2D). Among the major profibrogenic genes, real-time RT-PCR study revealed that hepatic expression of *Ctgf* was significantly higher in the knockout mice than in the control littermates (Figure 2E). Although *Tgfb1* and *Pdgfb* gene expression was slightly higher in the knockout mice than in the control litter-

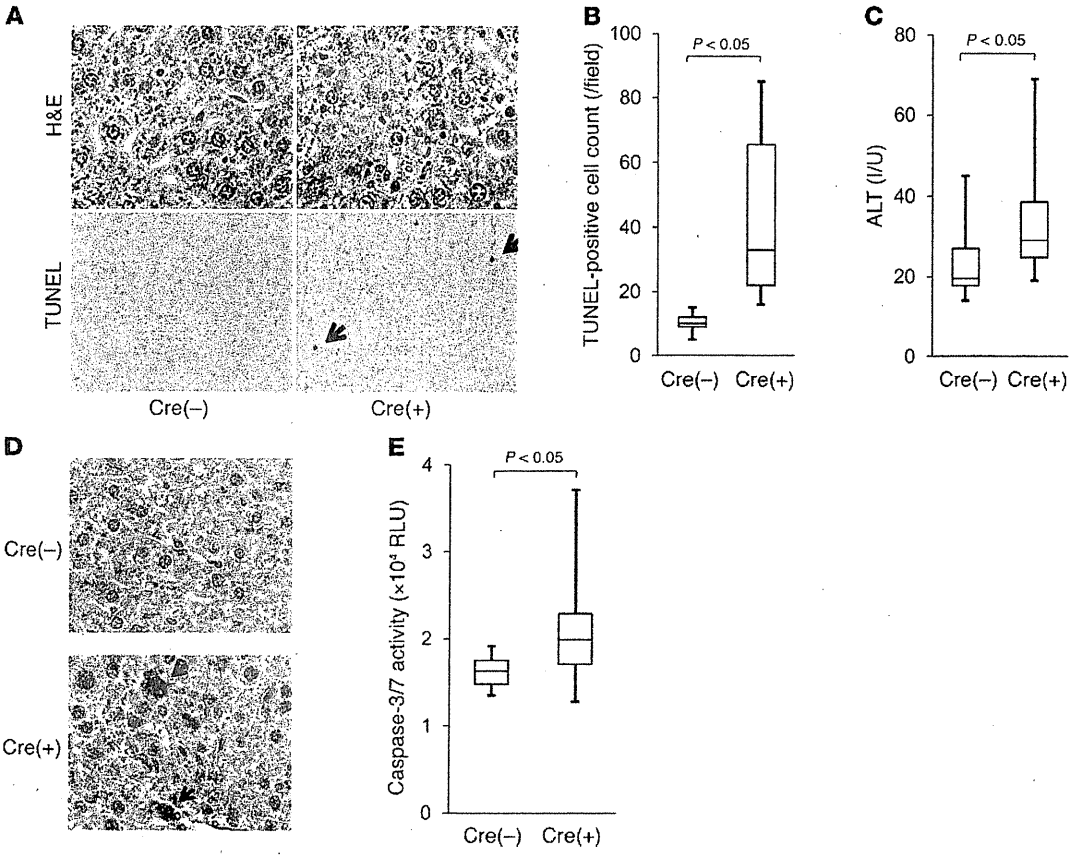

Figure 3

Hepatocyte-specific *Mdm2* deletion induces modest hepatocyte apoptosis. (**A**–**E**) *Mdm2*$^{fl/fl}$*alb-cre* [Cre(+)] mice and *Mdm2*$^{fl/fl}$ [Cre(–)] mice were examined at 6–8 weeks of age; more than 6 mice per group. (**A**) Hepatocyte apoptosis was evaluated by H&E staining and TUNEL staining of liver sections; black arrows indicate TUNEL-positive cells. Original magnification, upper panels, ×400; lower panels, ×200. (**B**) TUNEL-positive cell counts of liver sections. (**C**) Serum levels of ALT. (**D**) Expression of cleaved caspase-3 protein in the liver sections was assessed by immunohistochemistry; black arrows indicate cleaved caspase-3–positive cells. Original magnification, ×400. (**E**) Serum caspase-3/7 activity. RLU, relative light units.

mates, the difference was not significant (Supplemental Figure 3). These findings indicated that hepatocyte-specific *Mdm2* deletion led to spontaneous liver fibrosis with an increase in hepatic *Ctgf* gene expression. Activated hepatic stellate cells (HSCs), which express myogenic markers such as α-SMA, are major collagen-producing cells in the injured liver (19). We thus examined whether activated HSCs were involved in the spontaneous fibrosis of the knockout mice. Real time RT-PCR demonstrated that hepatic expression of the α-SMA gene *Acta2* was significantly higher in the knockout mice than in control littermates (Figure 2F), and immunohistochemical study revealed that α-SMA–positive cells increased in the liver of the knockout mice (Figure 2G), indicating that activated HSCs increased in the liver of the knockout mice. Liver fibrosis is known to be regulated by a fine balance between fibrogenesis and fibrinolysis, with activated HSCs playing a central role (19, 20). Real-time RT-PCR study showed that expression of fibrinolysis-related genes such as *Mmp2*, *Mmp14*, and *Timp1*, which are mainly produced from activated HSCs, also increased and was significantly higher in the knockout mice than in the control littermates (Figure 2H). These findings suggested the involvement of activated HSCs in regulation of the fibrosis phenotype in liver of the knockout mice.

Hepatocyte-specific Mdm2 deletion induces modest apoptosis, but regenerative capacity remains normal. p53 activation is known to induce apoptosis, cell-cycle arrest, and senescence in a variety of tissues (1). We examined apoptotic phenotypes in liver of the knockout mice. H&E staining of liver tissue revealed that a small number of hepatocytes with chromatin condensation and cytosolic shrinkage were scattered in the liver lobules of the knockout mice, with mild hepatic infiltration of inflammatory cells (Figure 3A). TUNEL staining of the liver tissue revealed an increase in TUNEL-positive cells in the knockout mice compared with the control littermates (Figure 3, A and B). Consistent with these histological observations, the levels of serum alanine aminotransferase (ALT), an indicator of liver injury, were slightly but significantly higher in the knockout mice than in the control littermates (Figure 3C). We also found that cleaved caspase-3, an active form of caspase-3, appeared in scattered hepatocytes of the knockout mice (Figure 3D), and that serum caspase-3/7 activity, which can be used as an indicator of hepatocyte apoptosis (21, 22), was significantly higher in the knockout mice than in the control littermates (Figure 3E). These findings indicated that hepatocyte-specific deletion of *Mdm2* led to a modest increase in spontaneous hepatocyte apoptosis. Next, we investigated the regenerative status of the liver upon 70% partial

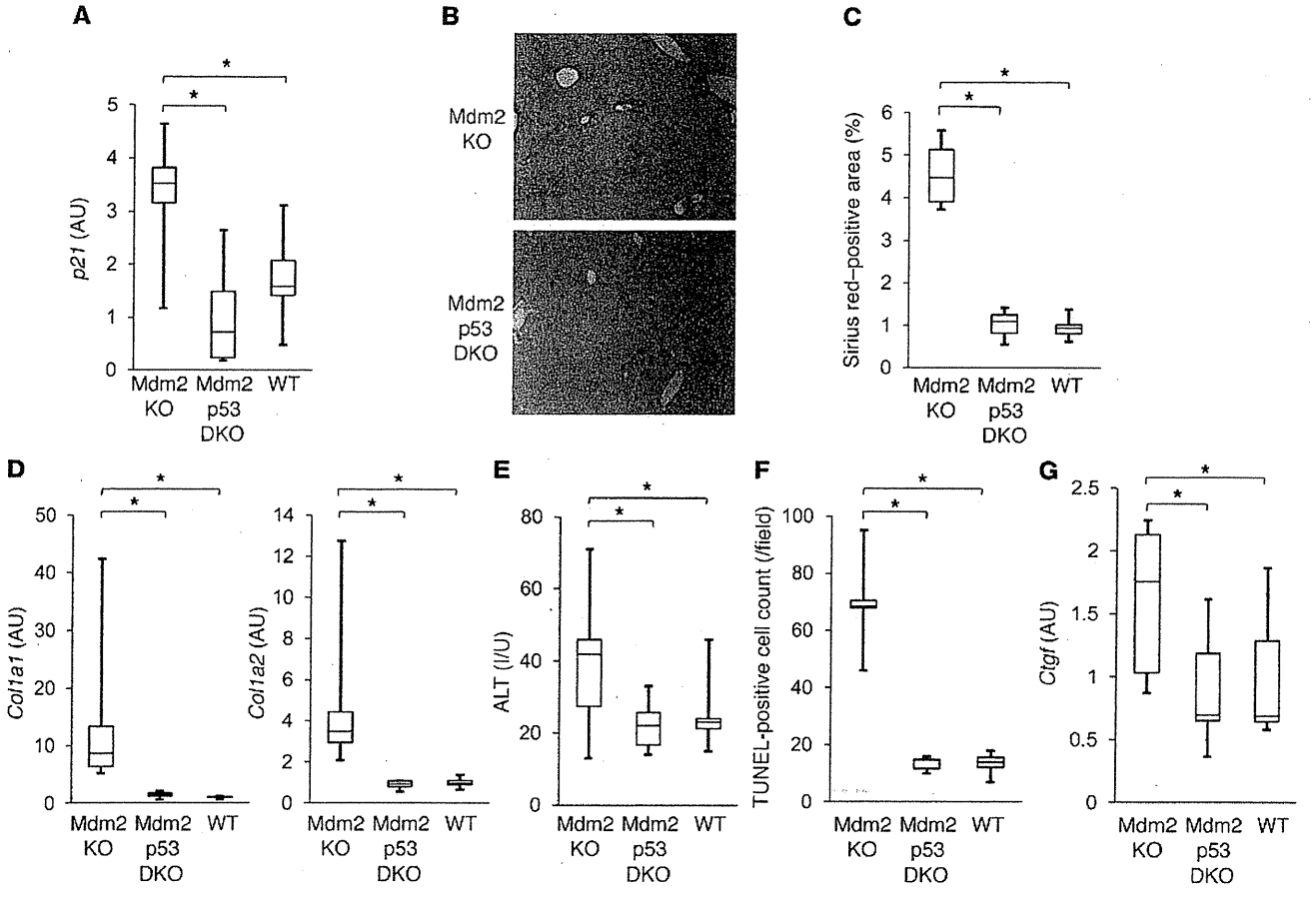

Figure 4

Spontaneous liver fibrosis in hepatocyte-specific Mdm2-knockout mice is completely abolished in a hepatocyte-specific p53-knockout background. (**A–G**) Offspring from mating of *Mdm2*$^{fl/fl}$*Trp53*$^{fl/+}$*alb-cre* mice and *Mdm2*$^{fl/fl}$*Trp53*$^{fl/+}$ mice were analyzed at 6 weeks of age; more than 5 mice per group. Mdm2 KO, *Mdm2*$^{fl/fl}$*Trp53*$^{+/+}$*alb-cre*; Mdm2 p53 DKO, *Mdm2*$^{fl/fl}$*trp53*$^{fl/fl}$*alb-cre*; WT, *Mdm2*$^{fl/fl}$*Trp53*$^{fl/fl}$ or *Mdm2*$^{fl/fl}$*Trp53*$^{+/+}$; $^*P < 0.05$. (**A**) *p21* mRNA levels in the liver were determined by real-time RT-PCR. (**B**) Liver fibrosis was evaluated by picrosirius red staining of liver sections. Original magnification, ×100. (**C**) Sirius red–positive area of liver sections. (**D**) *Col1a1* and *Col1a2* mRNA levels in the liver were determined by real-time RT-PCR. (**E**) Serum levels of ALT. (**F**) Hepatocyte apoptosis was evaluated by TUNEL staining of liver sections. (**G**) *Ctgf* mRNA levels in the liver were determined by real-time RT-PCR. $^*P < 0.05$.

hepatectomy, a well-established model of liver regeneration (23), by hepatic BrdU uptake and H&E staining of the liver tissue. Upon partial hepatectomy, compensatory liver regeneration occurred in both groups compared with the sham operation group, and the difference between them was not significant (Supplemental Figure 4, A and B). Even at a later time point, upon hepatectomy, liver volume steadily recovered in both groups and did not differ between them (Supplemental Figure 4C). These results indicated that hepatocyte-specific Mdm2 deficiency did not affect the regenerative capacity of the liver of the knockout mice. Senescence-associated β-galactosidase staining of the liver sections was also performed and showed that senescent hepatocytes were not obvious in both groups at 6 weeks of age (Supplemental Figure 5).

Spontaneous liver fibrosis in hepatocyte-specific Mdm2-knockout mice is abolished in a hepatocyte-specific p53-knockout background. To investigate whether p53 activation in hepatocytes is responsible for the phenotypes observed in the Mdm2-knockout mice, we generated hepatocyte-specific Mdm2- and p53-double-knockout mice by crossing hepatocyte-specific Mdm2-knockout mice (*Mdm2*$^{fl/fl}$*alb-cre*) and p53 floxed mice (*Trp53*$^{fl/fl}$). After mating of *Mdm2*$^{fl/fl}$*Trp53*$^{fl/+}$*alb-cre* mice with *Mdm2*$^{fl/fl}$*Trp53*$^{fl/+}$ mice, hepatocyte-specific Mdm2- and p53-double-knockout mice (*Mdm2*$^{fl/fl}$*Trp53*$^{fl/fl}$*alb-cre*) were born at the expected Mendelian frequency and grew normally (Supplemental Figure 6). Levels of the *p21* gene, as the p53-regulated gene, were significantly lower in the hepatocyte-specific Mdm2- and p53-double-knockout mice than in the hepatocyte-specific Mdm2-knockout littermates (*Mdm2*$^{fl/fl}$*Trp53*$^{+/+}$*alb-cre*) and were not significantly different from those in wild-type littermates (*Mdm2*$^{fl/fl}$*Trp53*$^{+/+}$ *or Mdm2*$^{fl/fl}$*Trp53*$^{fl/fl}$) (Figure 4A). Picrosirius red staining of the liver tissue demonstrated that spontaneous liver fibrosis was completely abolished in the double-knockout mice (Figure 4B) and collagen deposition was significantly lower in the double-knockout mice than in the Mdm2-knockout littermates (Figure 4C). Type I collagen gene expression also significantly decreased in the double-knockout mice compared with the single-knockout mice and was not different from that in wild-type littermates when assessed by real-time RT-PCR (Figure 4D). These findings clearly demonstrated that the spontaneous liver fibrosis in the Mdm2-knockout mice was completely dependent on p53,

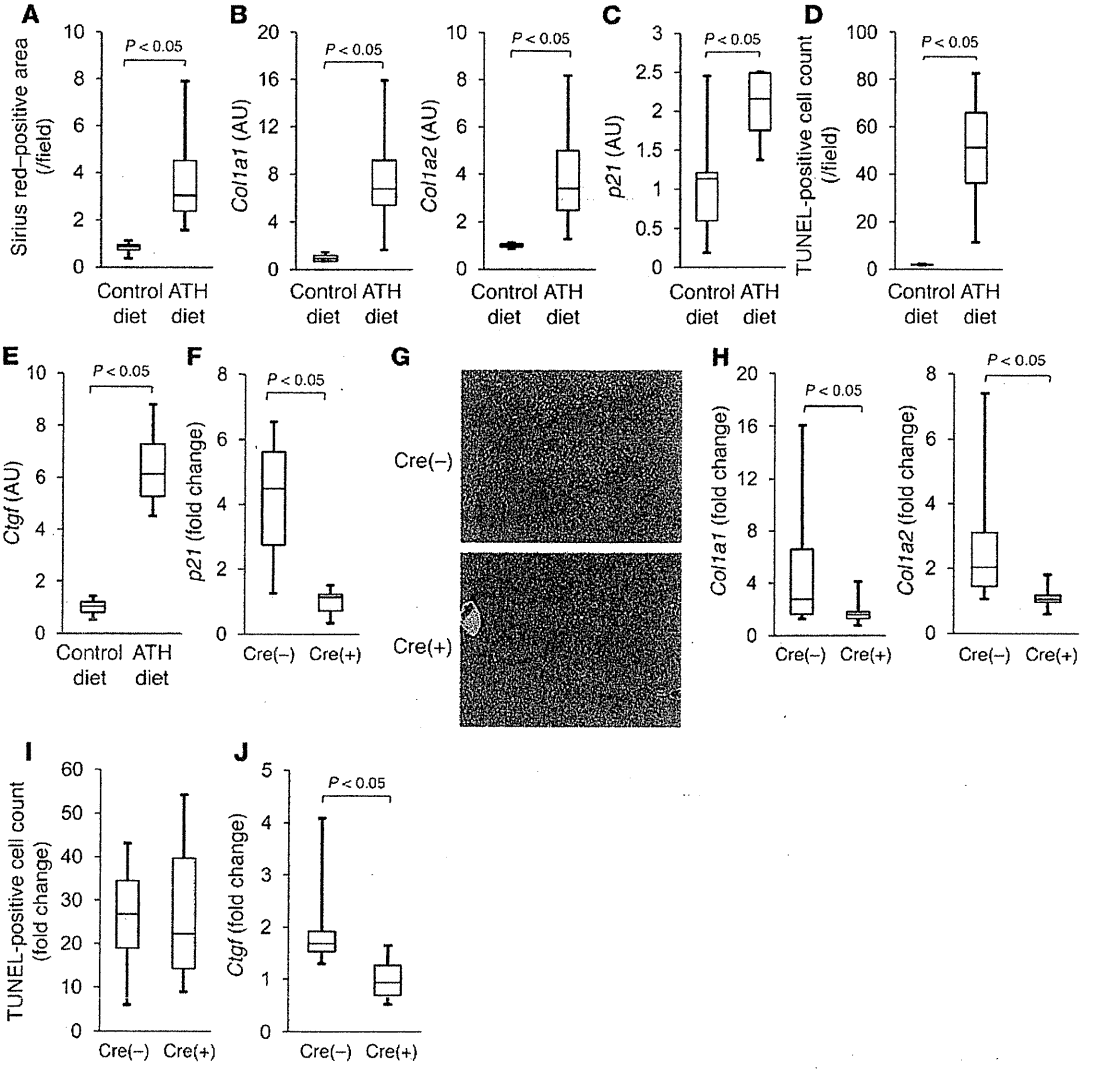

Figure 5

Hepatocyte-specific p53-knockout mice show alleviated liver fibrosis induced by ATH diet with suppression of the CTGF increase. (**A–E**) C57BL6/J mice were fed ATH diet or control diet for 4 weeks and then examined; 4 mice per group. (**A**) Liver fibrosis was evaluated by picrosirius red staining of liver sections. (**B**) *Col1a1* and *Col1a2* mRNA levels in the liver were determined by real-time RT-PCR. (**C**) *p21* mRNA levels in the liver were determined by real-time RT-PCR. (**D**) Hepatocyte apoptosis was evaluated by TUNEL staining of liver sections. (**E**) *Ctgf* mRNA levels in the liver were determined by real-time RT-PCR. (**F–J**) *Trp53*$^{fl/fl}$ [(Cre(–)] mice and *Trp53*$^{fl/fl}$*alb-cre* [Cre(+)] mice were fed ATH diet or control diet for 4 weeks and then examined; more than 6 mice per group; data are presented as fold change in the ATH diet group compared with the control diet group. (**F**) *p21* mRNA levels in the liver were determined by real-time RT-PCR. (**G**) Liver fibrosis was evaluated by picrosirius red staining of the liver sections. Original magnification, ×100. (**H**) *Col1a1* and *Col1a2* mRNA levels in the liver were determined by real-time RT-PCR. (**I**) Hepatocyte apoptosis was evaluated by TUNEL staining of liver sections. (**J**) *Ctgf* mRNA levels in the liver were determined by real-time RT-PCR.

indicating that endogenous p53 activation in hepatocytes causes spontaneous liver fibrosis. ALT levels were normalized in the double-knockout mice, with a significant decrease in TUNEL-positive cells in the liver (Figure 4, E and F). *Ctgf* gene expression was also significantly lower in the double-knockout mice than in the single-knockout mice and was not different from that in wild-type littermates (Figure 4G). These results indicated that hepatocyte p53 activation induced hepatocyte apoptosis and CTGF upregulation in the liver.

Hepatocyte-specific p53-knockout mice show alleviated liver fibrosis induced by ATH diet with suppression of CTGF increase. To investigate the involvement of p53 in liver fibrosis, we examined p53 activation in liver of wild-type mice fed an ATH diet, an experimental model of murine liver fibrosis (24, 25). After 4 weeks of ATH diet feeding, wild-type mice developed liver fibrosis as assessed by hepatic collagen deposition of picrosirius red staining, with upregulation of *Col1a1* and *Col1a2* gene expression (Figure 5, A and B). Regarding the p53-regulated genes, real-time RT-PCR analysis revealed that, in liver of the ATH diet–fed mice, *p21* gene expression levels rose and were significantly higher than those in liver of control diet–fed mice (Figure 5C). This finding suggested that p53 activation had occurred in the liver fibrosis induced by the ATH diet. TUNEL staining of the liver sections showed that hepatocyte

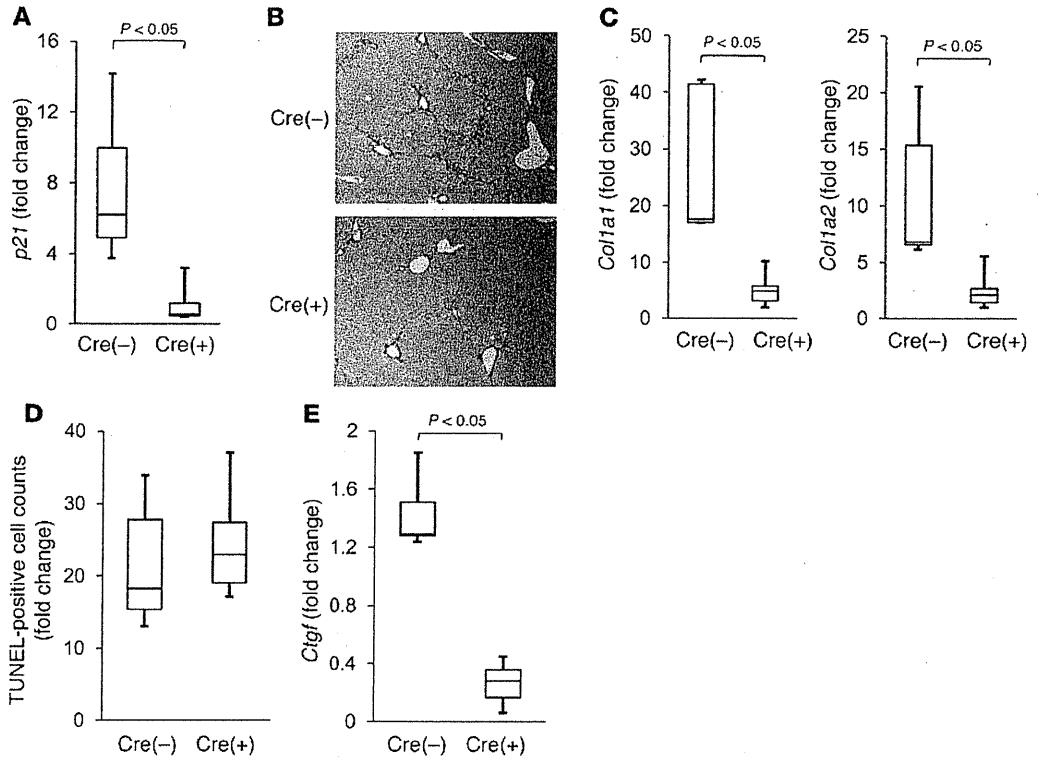

Figure 6

Hepatocyte-specific p53-knockout mice show alleviated liver fibrosis induced by TAA administration, with suppression of the CTGF increase. (**A**–**E**) *Trp53*$^{fl/fl}$ [Cre(–)] mice and *Trp53*$^{fl/fl}$*alb-cre* [Cre(+)] mice were given intraperitoneal injection of 200 mg/kg TAA 3 times per week for 6 weeks and then analyzed; 6 mice per group; data are presented as fold change in the TAA-treated group compared with the nontreated group. (**A**) *p21* mRNA levels in the liver were determined by real-time RT-PCR. Original magnification, ×100. (**B**) Liver fibrosis was evaluated by picrosirius red staining of the liver sections. (**C**) *Col1a1* and *Col1a2* mRNA levels in the liver were determined by real-time RT-PCR. (**D**) Hepatocyte apoptosis was evaluated by TUNEL staining of liver sections. (**E**) *Ctgf* mRNA levels in the liver were determined by real-time RT-PCR.

apoptosis significantly increased in ATH diet–fed mice compared with the control diet–fed mice (Figure 5D). Moreover, with this ATH diet, *Ctgf* gene expression significantly increased in the liver (Figure 5E). To investigate whether p53 activation was involved in the progression of liver fibrosis provoked by the ATH diet, the hepatocyte-specific p53-knockout mice (*Trp53*$^{fl/fl}$*alb-cre*) and the control littermates (*Trp53*$^{fl/fl}$) were fed the ATH diet or control diet, and then liver fibrosis was examined. After 4 weeks of feeding on the ATH diet, the *p21* gene was upregulated in the control littermates but not in the knockout mice, thus confirming p53 activation in hepatocytes in this fibrosis model (Figure 5F). Picrosirius red staining of the liver tissues revealed that liver fibrosis was alleviated in the knockout mice compared with the control littermates (Figure 5G). Real-time RT-PCR study demonstrated that the ATH diet–induced increase in *Col1a1* and *Col1a2* gene expression was significantly attenuated in the knockout mice compared with control littermates (Figure 5H). These results indicated that inhibition of p53 activation in hepatocytes alleviated the liver fibrosis caused by the ATH diet. With this ATH diet, hepatocyte apoptosis increased similarly in both groups compared with the control diet, and there was no significant difference between them in the increase, when assessed by TUNEL staining of the liver tissue (Figure 5I). This finding suggested that p53-dependent hepatocyte apoptosis was not much involved in this model. On the other hand, while the ATH diet upregulated *Ctgf* gene expression in the control littermates, this did not occur in the knockout mice (Figure 5J), suggesting that p53-mediated CTGF upregulation may be involved in the progression of liver fibrosis caused by the ATH diet.

Hepatocyte-specific p53-knockout mice show alleviated liver fibrosis induced by thioacetamide administration, with suppression of the increase in CTGF. To further investigate the involvement of p53 in another well-established model of liver fibrosis, we used repetitive intraperitoneal injection of thioacetamide (TAA) (26) to examine the hepatocyte-specific p53-knockout mice and control littermates. Upon 6 weeks of TAA administration, *p21* gene expression increased in the control littermates but not in the knockout mice, and there was a significant difference between them in its upregulation (Figure 6A). These findings suggested that p53 activation occurred in this fibrosis model as well. Picrosirius red staining of the liver sections revealed that liver fibrosis was alleviated in the knockout mice compared with control littermates (Figure 6B). Real-time RT-PCR study demonstrated that TAA-induced increases in *Col1a1* and *Col1a2* gene expression were significantly attenuated in the knockout mice compared with control littermates (Figure 6C). These results indicated that inhibition of p53 activation in hepatocytes alleviated TAA-induced liver fibrosis. TAA treatment increased hepatocyte apoptosis in both groups to a similar extent, as assessed by TUNEL staining of the liver tissue (Figure 6D). On the other hand, upon TAA treatment, there was a significant difference between them in the CTGF increase

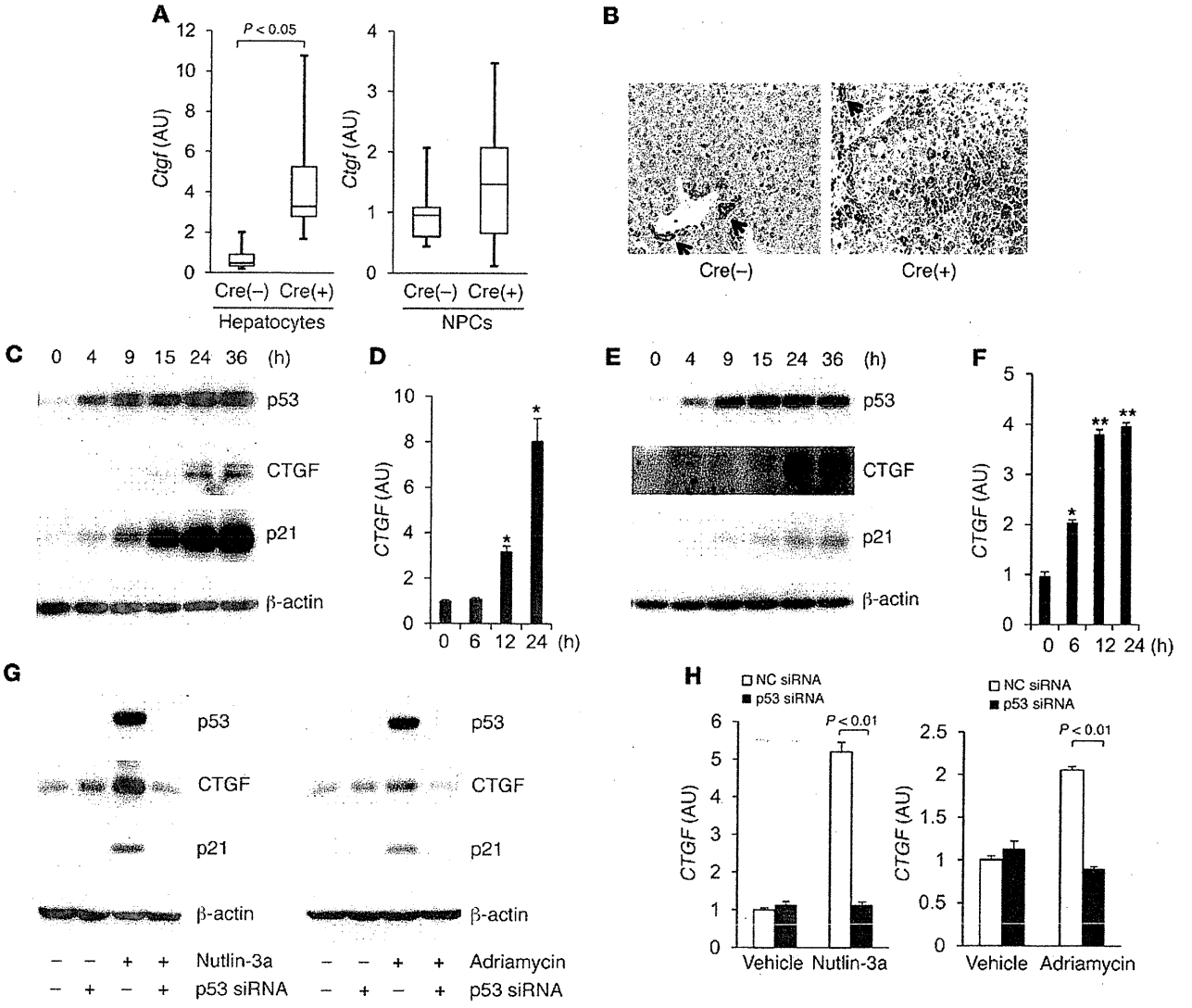

Figure 7

p53 regulates CTGF synthesis in hepatocytes. (**A**) Hepatocytes and NPCs were isolated from *Mdm2*$^{fl/fl}$ [Cre(–)] mice and *Mdm2*$^{fl/fl}$*alb-cre* [Cre(+)] mice by collagenase-pronase perfusion of the liver. *Ctgf* mRNA levels in the isolated hepatocytes (left panel) and NPCs (right panel) were determined by real-time RT-PCR; 4–6 mice per group. (**B**) Expression of CTGF protein in liver sections was assessed by immunohistochemistry; black arrows indicate cholangiocytes. Original magnification, ×200. (**C** and **D**) HepG2 cells (1.0×10^5) were treated with nutlin-3a (20 μM) or vehicle for the indicated time courses. (**C**) Western blot analysis of p53, CTGF, and p21 proteins. (**D**) Real-time RT-PCR analysis of *CTGF* mRNA expression; $n = 3$/group; $^*P < 0.01$ versus the other 3 groups. (**E** and **F**) HepG2 cells (1.0×10^5) were treated with Adriamycin (1 μM) or vehicle for indicated time courses. (**E**) Western blot analysis of p53, CTGF, and p21 proteins. (**F**) Real-time RT-PCR analysis of *CTGF* expression; $n = 3$/group; $^*P < 0.01$ versus the other 3 groups, $^{**}P < 0.01$ versus 0- and 6-hour groups. (**G** and **H**) HepG2 cells were transfected with *p53* siRNA or control siRNA for 3 days and then cultured for 24 hours with nutlin-3a (20 μM), Adriamycin (1 μM), or vehicle. (**G**) Western blot analysis of p53, CTGF and p21 proteins. (**H**) Real-time RT-PCR analysis of *CTGF* mRNA expression; $n = 3$/group, statistical analyses were performed by the paired *t* test.

(Figure 6E). These findings suggested that p53-mediated CTGF upregulation may be also involved in the progression of liver fibrosis provoked by TAA treatment.

p53 regulates CTGF synthesis in hepatocytes. We tried to identify the cells in which CTGF synthesis increased in the liver of hepatocyte-specific Mdm2-knockout mice. *Ctgf* gene expression in the hepatocytes of the knockout mice was significantly higher than in the control littermates (Figure 7A), while it did not significantly differ between them in the non-parenchymal cells (NPCs) (Figure 7A). Immunohistochemical examinations in the liver sections also revealed that CTGF was expressed in hepatocytes of the knockout mice, but not in those of control littermates (Figure 7B). On the other hand, CTGF was expressed in cholangiocytes of both groups of mice, but its levels were not much different between them. These findings suggested that p53 activation induced CTGF synthesis in murine hepatocytes. Next, to investigate the involvement of p53 in CTGF regulation in human hepatocytes, we performed an in vitro study using HepG2 cells, which are known to preserve wild-type p53 function (27). Administration of nutlin-3a into HepG2 cells led to time-dependent increases in p53 and p53-regulated gene